Imperial College London

Optimal control of dissipative quantum dynamics

Farhang Haddadfarshi

A thesis presented for the degree of
Doctor of Philosophy

Department of Physics
Imperial College London

January 2017

Supervised by Dr. Florian Mintert

Declaration

I hereby declare that this thesis is my own work. Material used from the published work of others has been acknowledged with citation listed in the bibliography.

London, January 2017
Farhang Haddadfarshi

Acknowledgements

There are respected individuals whom I would like to thank for their help and support during the development of this thesis. It is my pleasure to thank Dr. Florian Mintert, my supervisor, who provided valuable guidance, encouragement, direction, and feedbacks. Without his support and persistent help this dissertation would not have been possible. I would like to thank Jian Cui for our collaboration. I am grateful to him for sharing his knowledge of matrix representation of quantum states. Furthermore, I would like to acknowledge fruitful discussions with Winfried Hensinger, Matthias Keller, Klaus Mølmer, Cord Müller, Joe Randall, Tobias Schätz regarding the behaviour of noisy trapped ions. I would like to thank my colleagues whose presence and support during these times was precious. In particular, I would like to thank Albert, Bjoern, Federico, Bjoern B., Łukasz, Gregoire, Ludovico and Alejandro. I would like to thank my dear friends with whom I had a wonderful time during my research. In particular, I would like to thank Carlos, Elena and Francesca. I want especially to thank Sibilla for her support and company. Finally, I would like to thank my parents and my sister for all their support during these years and beyond.

Abstract

In this thesis, we develop a perturbative approximation for the solution of Lindblad master equations with time-dependent generators that satisfies the fundamental property of complete positivity, as essential for quantum simulations and optimal control of open quantum systems. By probing our method to several explicit examples we show that ensuring this property not only improves the accuracy of the perturbative approximation substantially, but also it permits to read off the effective dissipative processes . Subsequently, we design optimal entangling quantum gates for trapped ions mediated by a bus mode which is subject to decoherence. We show that suitably designed polychromatic control pulses, help to suppress the qubit-phonon entanglement substantially while maintaining the mediated interaction. This leads to a considerable reduction in the gate infidelity, in particular, for multi-qubit gates this yields a significant improvement in the gate performance.

Contents

List of Figures

Chapter 1

Introduction

The art of controlling the behaviour of quantum systems has transformed the realisation of universal quantum simulators into one of the most actively pursued goals in the field of quantum information. Simulation is a process of mapping the behaviour of one system onto another [1]. To simulate one quantum system using another, a method of controlling the dynamics of the quantum system is needed, so that the dynamics of the simulator can be transformed to mimic the behaviour of the system to be simulated. The methodology of control and manipulation of quantum systems is mainly based on the application of external, coherent radiation fields. As an example, this can be used to induce entanglement among trapped ions [2, 3].

In order to realise a desired behaviour of a quantum system to be simulated, one needs to identify proper driving field patterns which help to install and implement this desired dynamics in the quantum simulator. One approach to this identification is to obtain an analytical solution to the dynamics of the driven system, and optimising it with respect to the desired dynamics. This can be achieved using the methodology of series expansion [4, 5]. The central aspect of such approximations is the capacity to retain the algebraic structure of the system dynamics. That is the validity of the approximate solution is dependent on whether it incorpo-

rates the algebraic structure of the exact dynamics. Preserving unitarity which is the relevant algebraic structure in the analysis of closed quantum systems, can be achieved by resorting to series expansions based on exponential functions *e.g. Magnus expansion* [4]. Quantum simulations are not necessarily limited to closed quantum systems, and given the complexity in the analysis of the dynamics of quantum systems interacting with an environment, quantum simulators have proven to be effective tools to investigate the behaviour of open quantum systems [6]. Rather than unitarity, the fundamental properties of a driven open quantum system dynamics with a time-dependent generator is complete positivity. Developing an analytical scheme by which approximate maps satisfying this fundamental aspect can be constructed, would thus be a significant step towards control and simulation of open quantum systems.

One of the most successful hardwares investigated in the domain of quantum simulation are the well-controllable system of trapped ions, the potential of which for application of quantum information theory has been demonstrated abundantly [7–9]. Trapped ions have shown to be a promising candidate for the implementation of quantum logic gates [10, 11], which constitute the fundamental building block in the exploitation of quantum mechanical systems - execution of quantum algorithms, digital quantum simulations, quantum teleportation or precision sensing [12–16]; limitations in the obtained fidelity of quantum gates, however, is the hindering factor in harnessing the true potential of quantum mechanical systems. In the last years one could therefore witness dedicated efforts towards the increase of gate fidelities. Single qubit gates for trapped ions have been implemented with infidelities reaching 10^{-6} [17]; in contrast, the fidelities for entangling gates for two ions are substantially lower, in the range of 10^{-3} [18].

The qubits degree-of-freedom of the ions can be encoded in highly stable hyperfine or dressed states [19, 20] with very long coherence times; the central source of infidelity in entangling gates however, seems to be the

comparatively short coherence times of collective modes of vibration which play an essential role in mediating interaction amongst otherwise non-interacting qubits. Although designing an entangling scheme [3] that immunises the qubits from their collective bus mode decoherence has helped significantly towards the experimental implementation of two-qubit and multi-qubit entangling gates with reasonable fidelities [11, 21, 22], sensitivity to bus mode decoherence - induced by the environmental degrees of freedom - during the gate operation is still a limiting factor in the effort to reach fault tolerance.

The main focus of this thesis is to address the system of trapped ions in the context of the theory of open quantum systems. First, by developing a theoretical scheme through which the behaviour of driven open systems can be analysed, we provide a systematic framework to control and potentially simulate open quantum systems. Second, we will investigate the dynamics of quantum gates of trapped ions in the presence of motional decoherence from the open system dynamics perspective. By applying mathematical optimisation techniques, we will try to manipulate and control this dissipative dynamics, and eventually maintain the entangling gate fidelity. This thesis is composed in two parts. In part I (state of the art), we provide an introduction to the dynamics of open quantum systems as well as the dynamics of trapped ions. In part II (analysis of driven systems), we describe our investigation present the core results.

Part I is divided into three chapters. In chapter 2, we introduce the concept of open systems dynamics, and the notion of irreversibility. We review the state of the art formalism to model the behaviour of open quantum systems in terms of completely positive maps. In chapter 3, we review the mathematical methods based on series expansion to obtain analytical approximations to time-dependant differential equations. By applying two different classes of series, namely, Dyson series, and Magnus series, we assess their capacity in providing valid approximations to driven closed systems. In chapter 4, we provide an introduction the dynamics of trapped

ions and the behaviour of two distinct entangling schemes, namely, Ciarc-Zoller and Mølmer-Sørensen scheme.

Part II is divided into two chapters. In chapter 5, we describe the proposed correction scheme to the approximate solution of differential equation describing the dynamics of a driven open quantum system obtained using Magnus series. We evaluate the performance of the corrected series expansion in inducing valid approximations by investigating several driven open systems such as two-level systems, harmonic oscillator and lambda-systems. Finally in chapter 6, we study the entangling gates of trapped ions in presence of irreversible processes including thermalisation and dephasing. In particular we investigate the dynamics of dissipative Mølmer-Sørensen gate, and by applying optimal control techniques, we propose a polychromatic implementation of the scheme. Finally we assess the gate performance by evaluating the induced improvement of the polychromatic implementation compared with the conventional implementation of the gate.

Most of the results in this thesis can be found in the following publications

- FH, J. Cui and F. Mintert, *Phys. Rev. Lett.* **114**, 130402 (2015).

- FH and F. Mintert, *New J. Phys.* **18**, 123007 (2016).

Part I

State of the Art

Chapter 2

Open System Dynamics

2.1 Irreversible Dynamics

In reality no system is isolated from its surroundings - the environment - so every system is open to some extend. This often induces processes during which information flows from the system into the environment. As a result of this information loss the system dynamics cannot be simulated in terms of *reversible* maps *e.g.* unitary propagators. For a certain class of open systems there is no back-flow of information into the systems from the environment. The behaviour of such open quantum systems should be modelled in terms of *irreversible* maps, but first, one needs to understand the sufficient conditions under which this irreversible modelling of the system dynamics could be accurate, namely the Born-Markov approximation [23].

The fundamental concept is that the system interacts with an enormous environment through weak coupling. The weakness of the interaction ensures that the state of the environment is effectively unchanged and unaffected during the interaction; this is known as Born approximation. The enormity of the environment ensures that from one moment to the next the system effectively interacts with a different part of the environment and eventually the environment can be considered memoryless; this is known

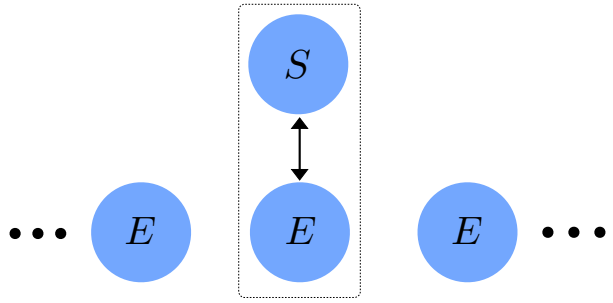

Figure 2.1: Markov approximation under which system is assumed to be interacting with an environment with large number of degrees of freedom such that any information flow from system into the environment gets effectively lost. In the case the environment can be considered memoryless.

as Markov approximation. An alternative way to understand Markov approximation is to consider the environment as a large set of degrees of freedom which interact with the system one after the other for a very short amount of time. Therefore, any influx of information from the system into the environment will be propagated within this enormous pool of degrees of freedom, and eventually will be lost without significant change in the state of the environment as if the system is constantly interacting with a fresh copy of the environment. (see Fig.(2.1))

In a regime in which the Born-Markov approximation can be considered accurate, one can derive a time-local differential equation for the density matrix of the open system alone. Such equation is typically refereed to as *master equation*. The behaviour of the whole systems (system + environment) ϱ_{SE} can be described in terms of von-Neumann equation

$$\dot{\varrho}_{SE}(t) = -i[\mathcal{H}_S + \mathcal{H}_E + \mathcal{W}, \varrho_{SE}(t)] \tag{2.1}$$

where $\mathcal{H}_S$, $\mathcal{H}_E$, and $\mathcal{W}$ correspond to the Hamiltonian of the open system,

the Hamiltonian of the environment and the system-environment coupling respectively. By considering the dynamics in the interaction picture with respect to the dynamics induced by $\mathcal{H}_S + \mathcal{H}_E$, one can obtain the following

$$\begin{aligned}\dot{\tilde{\varrho}}_{SE}(t) &= \dot{\mathcal{U}}(t)\varrho_{SE}(t)\mathcal{U}^\dagger(t) + \mathcal{U}(t)\dot{\varrho}_{SE}(t)\mathcal{U}^\dagger(t) + \mathcal{U}(t)\varrho_{SE}(t)\dot{\mathcal{U}}^\dagger(t) \\ &= i[\mathcal{H}_S + \mathcal{H}_E, \tilde{\varrho}_{SE}(t)] - i[\mathcal{H}_S + \mathcal{H}_E + \tilde{\mathcal{W}}(t), \tilde{\varrho}_{SE}(t)] \\ &= -i[\tilde{\mathcal{W}}(t), \tilde{\varrho}_{SE}(t)] \end{aligned} \tag{2.2}$$

with

$$\begin{aligned}\mathcal{U}(t) &= e^{-i(\mathcal{H}_S+\mathcal{H}_E)t}, \quad \text{and} \\ \tilde{\varrho} &= \mathcal{U}\varrho\mathcal{U}^\dagger.\end{aligned}$$

By solving Eq.(2.2) one obtains

$$\tilde{\varrho}_{SE}(t) = \tilde{\varrho}_{SE}(0) - i\int_0^t dt'[\tilde{\mathcal{W}}(t'), \tilde{\varrho}_{SE}(t')]. \tag{2.3}$$

Now by substituting this solution back into Eq.(2.2) one obtains the following differential equation

$$\dot{\tilde{\varrho}}_{SE}(t) = -i[\tilde{\mathcal{W}}(t), \tilde{\varrho}_{SE}(0)] - \int_0^t dt'[\tilde{\mathcal{W}}(t), [\tilde{\mathcal{W}}(t'), \tilde{\varrho}_{SE}(t')]]. \tag{2.4}$$

In order to obtain a differential equation for the reduced density matrix associated with the open system, ϱ_S only, one needs to trace over the environmental degrees of freedom

$$\dot{\tilde{\varrho}}_S(t) = -i\mathrm{Tr}_E[\tilde{\mathcal{W}}(t), \tilde{\varrho}_{SE}(0)] - \int_0^t dt'\mathrm{Tr}_E[\tilde{\mathcal{W}}(t), [\tilde{\mathcal{W}}(t'), \tilde{\varrho}_{SE}(t')]]. \tag{2.5}$$

For weakly interacting systems it is reasonable to assume that there are no correlations between the system and the environment, so that the density

matrix for the system and the environment can be written as

$$\tilde{\varrho}_{SE}(0) = \tilde{\varrho}_S(0) \otimes \tilde{\varrho}_E(0). \tag{2.6}$$

Let us consider the expectation value of the interaction Hamiltonian $\tilde{\mathcal{W}}$ with respect to the Hilbert space of the environment, $\langle \tilde{\mathcal{W}} \rangle_E$, which is assumed to be zero, *i.e.*

$$\mathrm{Tr}_E[\tilde{\mathcal{W}}(t)\tilde{\varrho}_{SE}(0)] = 0. \tag{2.7}$$

This is because there are no mean fields associated with the environment, since typically the environment is assumed to be in an equilibrium state *i.e.* vacuum or thermal state. The first crucial assumption is that since the open system interacts weakly with the environment, the state of the environment is slightly affected, so that it would be an acceptable approximation to replace $\tilde{\varrho}_{SE}(t')$ by $\tilde{\varrho}_S(t') \otimes \tilde{\varrho}_E(0)$ - Born approximation or the weak-coupling approximation - and this factorization assumption has an important role in deriving the evolution of the open system alone. Now the differential equation of the system density matrix reads

$$\dot{\tilde{\varrho}}_S(t) = -\int_0^t dt' \mathrm{Tr}_E[\tilde{\mathcal{W}}(t), [\tilde{\mathcal{W}}(t'), \tilde{\varrho}_S(t') \otimes \tilde{\varrho}_E(0)]]. \tag{2.8}$$

As one can see Eq.(2.8) is a differential equation with convolution; in other words, the behaviour of the open system at a specific time depends on the whole history of the state of the system. Such time-nonlocal equations are not easy to solve. It is therefore desirable to find time-local differential equation, that is, an equation in which the dynamics of the system at a specific time depends only on the system state at this instant of time. Therefore, one can perform the Markov approximation, in which the integrand $\tilde{\varrho}_S(t')$ is replaced by $\tilde{\varrho}_S(t)$, in which way, the dynamics for the density matrix of the open system at time t only depends on the present state $\tilde{\varrho}_S(t)$,

$$\dot{\tilde{\varrho}}_S(t) = -\int_0^t dt' \mathrm{Tr}_E[\tilde{\mathcal{W}}(t), [\tilde{\mathcal{W}}(t'), \tilde{\varrho}_S(t) \otimes \tilde{\varrho}_E(0)]]. \tag{2.9}$$

This is sometimes called the Redfield equation [23, 24]. The Redfield equation is time-local, but not Markovian since the dynamics of the open system depends on the explicit choice for the initial preparation at time $t = 0$. To obtain a Markovian master equation one substitutes the parameter t' with $t - t'$ in the integrand. The parameter t' encodes how far one can go backward in time to account for memory effects, which is equivalent to the time over which the correlations in the environment decays *e.g.* the correlation time τ_E. Under the Markov approximation these memory effects are short lived and the integrand decays quite rapidly. Thus one may replace the upper bound of the integration by infinity, and obtain a Markovian master equation for the open system dynamics

$$\dot{\tilde{\varrho}}_S(t) = -\int_0^\infty dt' \mathrm{Tr}_E[\tilde{\mathcal{W}}(t), [\tilde{\mathcal{W}}(t-t'), \tilde{\varrho}_S(t) \otimes \tilde{\varrho}_E(0)]]. \tag{2.10}$$

The timescale of the dynamics induced by this master equation is characterized by τ_S which is the time scale over which the open system relaxes due to interaction with the environment. For the Markov approximation to be accurate, the correlation time of the environment must be negligible compared with relaxation time of the open systems *e.g.* $\tau_E \ll \tau_S$.

2.2 Completely Positive Maps

The irreversible nature of the behaviour of an open system can be modelled in terms of a *semigroup* of transformations with a preferred direction in time [25]. As we discussed earlier there are physically plausible conditions under which the behaviour of the open system can be considered genuinely irreversible - the time scale for the open system should be large compared with the relaxation time of the environment and yet negligible compared with the recurrence time for the entirety of system and environment as a closed system. That is to say, there is only an intermediate time interval during which the semigroup modelling of the open system dynamics is

justified. In this section we would like to present an abstract overview of semigroup theory and its connection to dynamical maps.

2.2.1 Dynamical Semigroups

The mathematical theory of dynamical semigroups is based on the concept of positivity of operators and maps. An operator is called positive if and only if all of its eigenvalues are positive, and a positive map is a map from any positive operator to another positive operator. That is, the positivity of the operator is preserved under the action of a positive map. The positivity of density operator during the time evolution of the system for instance is an essential property of the dynamics which has to be preserved otherwise, the equations of motions will involve negative probabilities, and therefore, the positivity of the dynamical map (time evolution) is fundamental. Before introducing the dynamical semigroup structure from a mathematical point of view let us first have a quick introduction to an abstract but yet powerful mathematical structure called C*-algebra, which is the algebra of bounded operators on a complex Hilbert space with an involution such that $\| A^\dagger A \| = \| A \|^2$. By involution we mean the following adjoint properties

(i) $(A^\dagger)^\dagger = A$

(ii) $(AB)^\dagger = B^\dagger A^\dagger$

(iii) $(\alpha A + \beta B)^\dagger = \alpha^* A^\dagger + \beta^* B^\dagger$.

As one can see this algebra can be represented in terms of the algebra of complex matrices with †-map being the complex transposition of the matrices.

In the literature, there exist two classes of view on formulating the construct of dynamical semigroup. In the first class [26], a dynamical semigroup is defined as a one-parameter family of linear maps $\{\mathcal{E}_t\}$ acting on the elements of a C*-algebra $\mathscr{C}$ satisfying the following conditions

a - $\mathcal{E}_t > 0$; that is $\mathcal{E}_t$ is a positive map.

b -$\mathcal{E}_t \mathbb{I} = \mathbb{I}$; that is $\mathcal{E}_t$ is a unital (trace-preserving) map.

c - $\mathcal{E}_{t_1}.\mathcal{E}_{t_2} = \mathcal{E}_{t_1+t_2}$; that is $\mathcal{E}_t$ possesses the group property of closure.

d - $\forall A \in \mathscr{C} : ||\mathcal{E}_t A - A||_p \to 0$ as $t \downarrow 0$; that is $\mathcal{E}_t$ tends to identity as $t \to 0$ for $t > 0$.

Here $\| \circ \|_p$ denotes the operator p-norm, and can be mathematically represented as following [27]

$$\| \circ \|_p = \Big(\sum_j s_j^p(\circ) \Big)^{\frac{1}{p}} \tag{2.11}$$

where $s_j(\circ)$ denotes the jth eigenvalue of the operator $\circ$. For the special case $p = 1$ one obtains $\| \circ \|_1 = \text{Tr}[\sqrt{\circ\circ^\dagger}]$. The conditions c and d imply that the system dynamics is time-divisible and time-continuous respectively. The set forms a semigroup rather than a group structure because it does not necessarily include inverse elements. This algebraic structure formally models the idea of irreversible dynamics.

In the second class however, the positivity condition is not sufficient for a dynamical semigroup to have a physical interpretation for quantum systems, and a stronger condition of so-called complete positivity is required. Before presenting the second axiomatic definition of dynamical semigroups, let us understand the concept of complete positivity. It is always possible that the open system S might be correlated with another system B before the process modelled by $\mathcal{E}_t$ acts on system S. So the idea of complete positivity ensures that the total state of both systems remains a physical state with a positive density matrix. In other words, if the system S evolves and the system B does not, any initial density matrix of the combined system is mapped to another density matrix. In mathematical terms this means that the tensor product of the dynamical map with the identity map acting on the entirety of system and environment returns a positive operator

$$\mathcal{E}_t \otimes \mathbb{I}_{n\times n} > 0 \quad \text{for all } n. \tag{2.12}$$

That is to say, the extension of a positive operator to the higher dimensional space is mapped to a positive operator. By incorporating the notion

of complete positivity, a dynamical semigroup can be defined [25] as a one-parameter family of linear maps $\{\mathcal{E}_t\}$ acting on the elements of a C*-algebra $\mathscr{C}$ satisfying the following conditions

a - $\mathcal{E}_t$ is a completely positive map.

b - $\mathcal{E}_t\mathbb{I} = \mathbb{I}$; that is $\mathcal{E}_t$ is a unital.

c - $\mathcal{E}_{t_1}.\mathcal{E}_{t_2} = \mathcal{E}_{t_1+t_2}$; that is $\mathcal{E}_t$ possesses the group property of closure.

d - $\forall A \in \mathscr{C} : ||\mathcal{E}_t A - A||_p \to 0 \quad \text{as} \quad t \downarrow 0$; that is $\mathcal{E}_t$ tends to identity as $t \to 0$ for $t > 0$.

In this thesis, we will follow the latter view, and will take the concept of complete positivity as one of the fundamental aspects of dynamical semigroups. Next we will investigate the completely positive maps from the representation theory perspective - their mathematical representation in terms of linear transformations on the Hilbert space and their corresponding generators.

We would like to present the following theorem by Stinespring [28] on the mathematical form of completely positive maps

Steinespring factorization theorem. Let $\mathscr{A}$ be a C*-algebra and $\mathscr{H}$ be a Hilbert space, and let $\mathcal{E}$ be a linear map from $\mathscr{A}$ to operators on $\mathscr{H}$. Then a necessary and sufficient condition that $\mathcal{E}$ is of the form

$$\mathcal{E}(A) = V^\dagger \varrho(A) V \qquad \text{for all } A \in \mathscr{A} \tag{2.13}$$

where V is a bounded linear operator from $\mathscr{H}$ to the Hilbert space $\mathscr{K}$ and ϱ is a $*$-representation of $\mathscr{A}$ into operators on $\mathscr{K}$ is that $\mathcal{E}$ be completely positive. As a special case in which $\mathscr{H} = \mathscr{K}$, that is the dynamics of the systems at all times is described in terms of only one Hilbert space, it was shown [29] that $\mathcal{E}$ is a completely positive map if and only if it is of the form

$$\mathcal{E}(A) = \sum_j V_j^\dagger A V_j \qquad \text{for} A \in \mathcal{B}(\mathscr{H}), \tag{2.14}$$

where $\{V_j\}$ are bounded operators in the Hilbert space $\mathscr{H}$. This is often called Kraus representation or operator-sum representation of quantum channels. The operators $\{V_j\}$ encode the phenomenological description of the processes through which the open system interacts with the environment; so depending on the nature of such processes together with symmetry aspects of the system *e.g.* invariance under symmetry groups [30], one should be able to construct the relevant form of the completely positive map $\mathcal{E}$.

As we mentioned in the previous section, under Born-Markov approximation the behaviour of the open quantum system can be described in terms of an autonomous differential equation. Now given the most general form of the behaviour of the open system in Eq.(2.14), what is the most general form of such an autonomous equation? Alternatively, what is the most general mathematical form of the operator $\mathcal{L}$ given the following equation

$$\dot{\mathcal{E}} = \mathcal{L}\mathcal{E} \tag{2.15}$$

which is referred to as the *master equation*. By studying the mathematical structure of completely positive maps and their underlying algebraic properties, Lindblad [25] was able to show that the most general form of the generator of a completely positive map is of the form

$$\mathcal{L}[\circ] = \sum_j \mathcal{D}_{V_j}[\circ] \quad \text{with} \quad \mathcal{D}_{\hat{O}}[\circ] = \hat{O} \circ \hat{O}^\dagger - \frac{1}{2}\{\hat{O}^\dagger \hat{O}, \circ\}. \tag{2.16}$$

The set $\{V_j\}$ is called the set of Lindblad operators and as we pointed out earlier they represent the phenomenological description of the dissipative processes in the system. One can rewrite the generator $\mathcal{L}$ in terms of a complete basis of orthonormal operators $\{E_j\}, i = 1, 2, ..., N^2$, where N is dimension of the Hilbert space, and the orthonormality condition can be

expressed as

$$(E_i, E_j) \equiv \mathrm{Tr}_S\{E_i^\dagger E_j\} = \delta_{ij}. \tag{2.17}$$

For convenience one can choose $E_{N^2} = (1/N)^2\mathbb{I}$, so that other basis operators are traceless. In this basis one can write

$$V_j = \sum_{k=1}^{N^2} (V_j, E_k) E_k. \tag{2.18}$$

In this new basis the generator can be expressed as following

$$\mathcal{L}[\circ] = -i[\mathcal{H}, \circ] + \sum_{k,l=1}^{N^2-1} [\mathbb{C}]_{kl} (E_k \circ E_l^\dagger - \frac{1}{2}\{E_l^\dagger E_k, \circ\}). \tag{2.19}$$

where the Hermitian operator $\mathcal{H} = \sum_{j=1}^{N^2-1} i[\mathbb{C}]_{j,N^2}(E_j - E_j^\dagger)/2$ encodes the reversible part of the open system dynamics - von Neumann equation - and the second part of the Eq. (2.19) can be considered as the dissipative correction with $[\mathbb{C}]_{kl} = \sum_j (V_j, E_k)(V_j, E_l)^*$ being a self-adjoint positive semidefinite matrix for which the eigenvalues correspond to the dissipative rates. In order to see this, one can rewrite the coefficient matrix $\mathbb{C}$ in the diagonal form as following

$$[\mathbb{C}]_{kl} = [\sum_j \Gamma_j |\Phi_j\rangle\langle\Phi_j|]_{kl} = \sum_j \Gamma_j \langle k|\Phi_j\rangle\langle\Phi_j|l\rangle, \tag{2.20}$$

in terms of which Eq.(2.19) can be written as

$$\begin{aligned} \mathcal{L}[\circ] &= -i[\mathcal{H}, \circ] + \sum_j \Gamma_j \mathcal{D}_{\sum_{k=1}^{N^2-1}\langle\Phi_j|k\rangle E_k}[\circ] \\ &= -i[\mathcal{H}, \circ] + \sum_j \Gamma_j \mathcal{D}_{F_j}[\circ]. \end{aligned} \tag{2.21}$$

The coefficients $\{\Gamma_j\}$ can be regarded as the rate at which dissipative processes $\{F_j\}$ occur. This equation expresses the dynamics of an open sys-

tems in terms of a purely reversible and a purely irreversible section.

2.3 Simulation of Open Systems

Utilizing a well controllable quantum system to mimic the behaviour of another less accessible quantum system - *quantum simulation* - can be conceived in terms of the following scheme [31] : mapping the generator of the simulated system behaviour to an algebraically equivalent, but physically quite different generator, so that the behaviour of the original system could be *emulated*. The information of interest regarding the emulated system can be extracted via performing measurements on the second system (simulator) as shown in Fig.(2.2).

An important aspect of quantum simulation is being able to control the behaviour of the simulator, what is known as *quantum control*. In general,

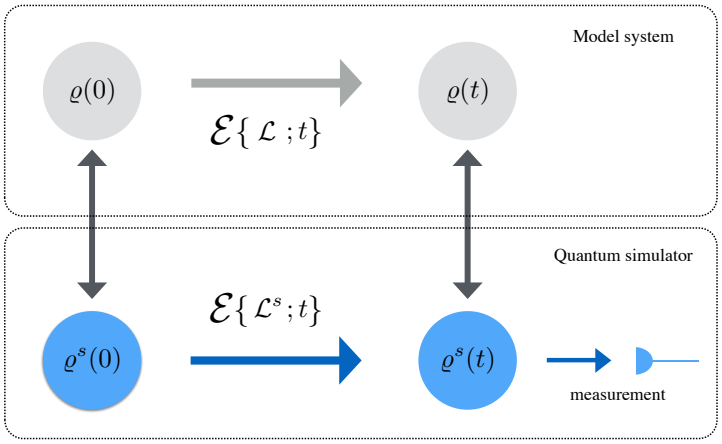

Figure 2.2: The main phases of quantum simulation consists of state preparation, time evolution over a certain time and carrying out measurement on the final state to extract the physical information of interest.

the control theory of quantum systems is the concept of making a quantum system behave in a more desirable way. This can be achieved by modify the system dynamics through applying time-dependent control functions to the underlying Hamiltonian *e.g.* illuminate the system using external radiation fields. The design of such control functions by utilising pulse-shaping techniques leads to the realisation of the objective system behaviour. In order to identify the proper control scheme that helps to design these time-dependent control functions, one must be able to represent the dynamics of the driven system, which then can be compared and optimised with respect to the target dynamics, and typically these representation can be obtained by utilising the methodology of series expansion. Most commonly, this implies a series expansion of the solution for the differential equation

$$\dot{\mathcal{E}}(t) = \mathcal{L}(t)\mathcal{E}(t) \tag{2.22}$$

with the time-depenent generator $\mathcal{L}(t)$,

$$\mathcal{L}(t)[\circ] \equiv \sum_{j=1}^{N^2} \Gamma_j(t)\mathcal{D}_{F_j}[\circ]. \tag{2.23}$$

As one can see the control functions can be implanted within the Γ-matirx, which encodes the corresponding modulated rates with which the processes $\{F_j\}$ occur; in the simulation of open system dynamics, however, one needs to bear in mind that the control functions should satisfy the condition under which the validity of the semigroup formalism of the open system behaviour is maintained. In other words, the applied control scheme should not undermine the premise of Markovianity of the environment. This means that the control rates should be negligible compared with the correlation frequency of the environment *e.g.* $\Gamma_j(t) \ll \tau_E^{-1}$ [32]. By consid-

ering the generator in terms of the reversible and irreversible parts,

$$\mathcal{L}(t)[\circ] \equiv -i[\mathcal{H}(t), \circ] + \sum_{j=1}^{N^2-1} \Gamma_j(t)\mathcal{D}_{F_j}[\circ] \tag{2.24}$$

in order to control the system behaviour, one thus can either engineer the coherent part of the dynamics by having a set of suitably chosen Hamiltonians, or, one can equally engineer the dissipative part of the dynamics by having a set of processes $\{F_j\}$ with suitably chosen rates $\Gamma_j(t)$.

As we mentioned earlier, the system dynamics can be represented in terms of a series expansion *e.g.*

$$\mathcal{E}(t) \sim \sum_j a_j \mathcal{A}^{(j)}, \tag{2.25}$$

where the right-hand side of the Eq.(2.25) is an asymptotic series generated by $\mathcal{L}(t)$. Such an expansion is typically obtained using *Dyson series* [5], *Magnus series* [4] or variations thereof [33–35]. The approximated dynamics $\mathcal{E}(t)$ then can be compared with the desired dynamics $\mathcal{E}_d(t)$, and the distance between the two maps can be minimized

$$\min_{\{\mathcal{H}(t),\Gamma_j(t)\}} ||\mathcal{E}(t) - \mathcal{E}_d(t)||. \tag{2.26}$$

This can be achieved by incorporating suitably chosen control functions $\mathcal{H}(t)$ and $\Gamma_j(t)$ over which the mathematical optimisation methods can be performed.

Chapter 3

Series Expansion

3.1 Dyson Series

As we mentioned in the previous chapter, the behaviour of a driven open quantum system can be represented in terms of an asymptotic series given in Eq.(2.25). One of the methods to construct such series is the method of Dyson series. Let us consider the following problem of obtaining an analytical solution to a first-order differential equation with a time-dependent generator

$$\dot{\mathcal{E}} = \mathcal{L}(t)\mathcal{E} \tag{3.1}$$

which may represent the master equation describing the behaviour of a driven open quantum system. Because of the time-dependency of the generator the exact solution can not be deduced, and therefore, one needs to resort to various types of approximations, which is mostly based on the methodology of series expansion [5, 36] - the representation of an *unknown* function in terms of a series of *known* functions. The master equation as well as the initial condition $\mathcal{E}_{t=0} = \mathbb{I}$ is apparently satisfied by the solution of the integral equation

$$\mathcal{E}(t) = \mathbb{I} + \int_0^t dt' \mathcal{L}(t')\mathcal{E}(t'). \tag{3.2}$$

By iteration of this integral equation, one obtains a series expansion for the map $\mathcal{E}(t)$ in powers of $\mathcal{L}$

$$\begin{aligned}\mathcal{E}(t) &= \mathbb{I} + \int_0^t dt' \mathcal{L}(t') + \int_0^t dt' \int_0^{t'} dt'' \mathcal{L}(t')\mathcal{L}(t'') \\ &+ \int_0^t dt' \int_0^{t'} dt'' \int_0^{t''} dt''' \mathcal{L}(t')\mathcal{L}(t'')\mathcal{L}(t''') + ... \end{aligned} \tag{3.3}$$

One can define the *time-ordering product* [5, 36] $\mathcal{T}$ of any time-dependent operator as the product with factors arranged so that the operator with the latest time-argument is placed leftmost, the next-latest next to the leftmost, and so on. For example

$$\begin{aligned}\mathcal{T}\{\mathcal{L}(t)\} &= \mathcal{L}(t) \\ \mathcal{T}\{\mathcal{L}(t_1)\mathcal{L}(t_2)\} &= \theta(t_1 - t_2)\mathcal{L}(t_1)\mathcal{L}(t_2) + \theta(t_2 - t_1)\mathcal{L}(t_2\mathcal{L}(t_1) \\ \mathcal{T}\{\mathcal{L}(t_1)...\mathcal{L}(t_n)\} &= \sum_p \theta(t_{p_1} > ... > t_{p_n})\mathcal{L}(t_{p_1})...\mathcal{L}(t_{p_2}). \end{aligned} \tag{3.4}$$

where θ is the Heaviside step function, and the summation is over all the $n!$ permutations of the $\mathcal{L}$s.

By adapting this notation, Eq.(3.3) can be written as

$$\mathcal{E}(t) = \mathbb{I} + \sum_n \frac{1}{n!} \int_0^t dt_1 \int_0^t dt_2 ... \int_0^t dt_n \mathcal{T}\{\mathcal{L}(t_1)\mathcal{L}(t_2)...\mathcal{L}(t_n)\}. \tag{3.5}$$

This is known as *Dyson series*[5]; in general this series does not converge, but it can be understood and utilised in terms of asymptotic analyses. Dyson series is a very powerful tool to study scattering theory and to analyse processes in terms of Feynman diagrams [36], but in the domain of quantum information theory where one is interested in unitary (reversible) transformations, it is problematic. Let us consider a closed system for which the

system behaviour can be encoded in the time-dependent generator

$$\mathcal{L}(t)[\circ] = -i[\mathcal{H}(t), \circ] \tag{3.6}$$

where $\mathcal{H}(t)$ is the system Hamiltonian. Since the system is closed, its behaviour must be reversible, in other words, the solution of the master equation must be a unitary map. On the other hand, because of the time dependency of the generator one needs to apply the Dyson series in order to obtain an approximate solution as following

$$\mathcal{E}(t)[\circ] = \mathbb{I} - i\int_0^t dt'[\mathcal{H}(t'), \circ] - \frac{1}{2}\int_0^t dt' \int_0^{t'} dt''[\mathcal{H}(t'), [\mathcal{H}(t''), \circ]] + ... \tag{3.7}$$

By truncating this series expansion at any order of the approximation, one can see that the resulted approximate solution does not preserve the condition of unitarity,

$$\mathcal{E}\mathcal{E}^\dagger \neq 1 \tag{3.8}$$

that is to say, the approximate solution does not respect the unitarity of the system dynamics which is the artifact of the series truncation in the approximation. This is often a disadvantage in the field of quantum information processing [37] where usually quantum gates are encoded in terms of unitary transformations. In mathematical analysis one way to bypass this problem is to resort to an alternative approximation based on series expansion known as *Magnus series* which preserves the unitarity of the approximate map at any order of the approximation as we will discuss in the following section.

3.2 Magnus Series

The *Magnus series* [4, 38, 39] provides an exponential representation to the solution of the first-order differential equation $\dot{\mathcal{E}} = \mathcal{L}(t)\mathcal{E}$. The prominent

aspect of this series expansion is that it leads to approximate solutions that maintain some qualitative characteristics that are guaranteed by the underlying algebraic structure for the physical systems *e.g.* symplectic or unitary character of the time evolution operator for closed systems. Wilhelm Magnus (1954) derived the following series with which one can generate the solution to the master equation

$$\mathcal{E}(t) = e^{\mathfrak{L}(t)} = e^{\mathfrak{L}^{(1)}(t)+\mathfrak{L}^{(2)}(t)+\ldots} \tag{3.9}$$

with the elements corresponding to different orders of the approximation can deduced recursively

$$\begin{aligned}
\mathfrak{L}^{(1)}(t) &= \int_0^t dt' \mathcal{L}(t'), \\
\mathfrak{L}^{(2)}(t) &= \frac{1}{2}\int_0^t dt' [\mathcal{L}(t'), \mathfrak{L}^{(1)}(t')], \\
\mathfrak{L}^{(3)}(t) &= \frac{1}{2}\int_0^t dt' [\mathcal{L}(t'), \mathfrak{L}^{(2)}(t')] + \frac{1}{12}\int_0^t dt' [[\mathcal{L}(t'), \mathfrak{L}^{(1)}(t')], \mathfrak{L}^{(1)}(t')], \\
&\ldots
\end{aligned} \tag{3.10}$$

Since the approximate solution is represented in terms of an exponential function, it consists of higher order terms that are not necessarily valid, but it is exactly because of these higher order terms that approximation exhibit the very characteristics that are imposed by the algebraic structure such as unitarity for closed systems. Now by constructing the Magnus series for a closed system with $\mathcal{L}[\circ] = -i[\mathcal{H}, \circ]$ one obtains

$$\begin{aligned}
\mathcal{E}(t)[\circ] &= \exp\Big(-i\int_0^t dt' [\mathcal{H}(t'), \circ] \\
&- \frac{1}{2}\int_0^t dt' \int_0^{t'} dt'' [\mathcal{H}(t'), [\mathcal{H}(t''), \circ]] - [\mathcal{H}(t''), [\mathcal{H}(t'), \circ]] + \ldots\Big).
\end{aligned} \tag{3.11}$$

Due to the exponential form of the approximation, one can easily check that the truncated series expansion satisfies the fundamental property of

unitarity, $\mathcal{E}\mathcal{E}^{\dagger} = \mathbb{I}$.
By considering $\mathcal{E} = e^{\sum_j \mathfrak{M}^{(j)}} = \mathbb{I} + \sum_j \mathfrak{D}^{(j)}$, where $\mathfrak{M}$ and $\mathfrak{D}$ correspond to the terms in Magnus and Dyson series respectively, one can obtain the following relations

$$\begin{aligned}
\mathfrak{M}^{(1)} &= \mathfrak{D}^{(1)} \\
\mathfrak{M}^{(2)} &= \mathfrak{D}^{(2)} - (1/2)\mathfrak{D}^{(1)}\mathfrak{D}^{(1)} \\
\mathfrak{M}^{(3)} &= \mathfrak{D}^{(3)} - (1/2)(\mathfrak{D}^{(1)}\mathfrak{D}^{(2)} + \mathfrak{D}^{(2)}\mathfrak{D}^{(1)}) + (1/3)\mathfrak{D}^{(1)}\mathfrak{D}^{(1)}\mathfrak{D}^{(1)} \\
&\ldots
\end{aligned} \tag{3.12}$$

One should note that the both series expansions coincide at every order of the approximation, and therefore they are both valid up to the order that one is interested; the Magnus series however, incorporates higher order terms that account for the preservation of the algebraic structure of the system.

3.3 Graph Analysis

An alternative approach to construct the Magnus series is to adapt the graph theoretical representation - associating each term in the series with a *binary rooted tree*[38, 39]. In this representation the generator $\mathcal{L}$ is associated with a tree of order one, consisting of a single vertex; integration is encoded in the language of graph theory by appending a edge to the root of a tree, whereby the other end of the edge becomes the root; commutation is encoded by joining the roots of two trees to a new root. Therefore

where the tree section encloses in the loop is constructed in the previous order of the approximation emphasizing the recursive nature of the series expansion. Now the Magnus series can be constructed by simply attaching these elemental terms in various combinations constrained by the number of vertices corresponding to the order of approximation. By following this construction algorithm, the Magnus series can be written in the following compact form

$$\mathfrak{M}(t) = \sum_{j=1}^{\infty} \sum_{k \in \mathfrak{T}_j} \alpha_j^{(k)} \mathfrak{T}_j^{(k)} \tag{3.13}$$

where $\mathfrak{T}_j$ is the set of all binary trees of order j, and the coefficients α are related to the sequence $\{f_m\}_{m \in \mathbb{Z}^+}$ as shown in the table below [38] with

$$\sum_{m=0}^{\infty} f_m z^m = \sum_{m=0}^{\infty} \frac{B_m}{m!} z^m + z = 1 + \frac{1}{2}z + \frac{1}{12}z^2 - \frac{1}{720}z^4 + ... \tag{3.14}$$

where $\{B_m\}_{m \in \mathbb{Z}^+}$ denotes the *Bernoulli numbers*. The coefficients can be constructed by simply reading the graph pattern; that is every term in the series either can be constructed by merging previous graphs in which case the coefficient is the multiplication of previous coefficients corresponding to the constituent graphs or is just a new pattern in which case the new

Table 3.1: Graph representation of the terms in Magnus series up to the third order, $\mathfrak{T}$ and the corresponding coefficients α

order	tree	coefficient
$\mathfrak{T}_1$		1
$\mathfrak{T}_2$		f_1
$\mathfrak{T}_3$	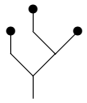	f_2
$\mathfrak{T}_3$	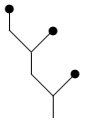	f_1^2

coefficient can simply be read from the Eq.(3.14). Therefore, the series obtained in the Eq.(3.10) can be visually represented as following

$\mathfrak{M} =$ 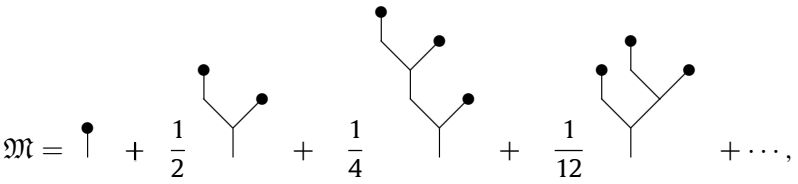 $+\cdots,$

As one can see the rule for constructing the series expansion at the every order of the approximation j is based on the combinatorics - combin-

ing possible ways of composing binary trees with j vertices and j edges weighted by coefficients constructed in terms of Bernoulli numbers.

The last point regarding Magnus series that needs to be addressed is the convergence of the series which has been investigated extensively in the literature in terms of the radius of convergence; here however, we would like to mentioned that there exist a theorem [39] which states that the Magnus series

$$\mathfrak{L}(t) = \sum_j \mathfrak{L}^{(j)} \tag{3.15}$$

converges in the interval $t \in [0, T)$ such that

$$\int_0^T ds \parallel \mathcal{L}(s)[\circ] \parallel_2 < \pi, \tag{3.16}$$

where $\mathfrak{L}(t)$ satisfies $e^{\mathfrak{L}(t)} = \mathcal{E}(t)$. As we will discuss in part II we will not be concerned with this criterion of convergence as we will be investigating the open systems in the fast driving regimes under stroboscopic perspective in which case every term in the series expansion will be multiplied by a perturbation parameter inversely proportional to the powers of the driving frequency

$$\mathfrak{L}(t) = \sum_j \frac{\mathcal{A}^{(j)}}{\omega^j} \tag{3.17}$$

where ω denotes the driving frequency. As one can see in the regime of fast driving *e.g.* $\omega \gg \parallel \mathcal{A}^{(1)} \parallel$, the convergence of this series expansion is ensured.

Chapter 4

Logic Gates

4.1 Trapped Ions

The potential of confining a collection of charged particles within a particular configuration of electromagnetic fields for the application of quantum computation has been demonstrated abundantly in terms of satisfying the most elementary criteria of a quantum computer, namely, state preparation, gate operation and read-out [40]. The behaviour of a single trapped ion can be mathematically modelled by incorporating two sets of degrees of freedom - the internal degree of freedom encoding the spin state of the ion, and the external degree of freedom encoding the vibration of the ion within the trap zone - which to a high degree of approximation can be represented by a two-level system and a harmonic oscillator respectively as illustrated in Fig.(4.1).

The Hamiltonian of a single trapped ion driven by a radiation field can be written as [41]

$$\mathcal{H} = \mathcal{H}_s + \mathcal{H}_p + \mathcal{H}_r \tag{4.1}$$

with

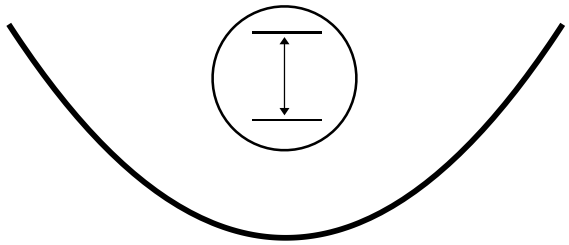

Figure 4.1: Scheme of a single trapped ions - a two-level system positioned within a harmonic trap.

$$\begin{aligned} \mathcal{H}_s &= \hbar\frac{\omega_{eg}}{2}\sigma_z \\ \mathcal{H}_p &= \hbar\nu a^\dagger a \\ \mathcal{H}_r &= \hbar\frac{\Omega}{2}(\sigma_+ e^{i[\eta(a+a^\dagger)-\omega t]} + \text{H.c.}) \end{aligned} \tag{4.2}$$

in terms of the resonance frequency ω_{eg} of the bare two-level system, the resonance frequency ν of the bare harmonic oscillator, the driving frequency ω and the Rabi frequency Ω of the driving radiation field, the creation and annihilation operators $\{a, a^\dagger\}$ of the harmonic oscillator excitations, the set of Pauli matrices $\{\sigma_j\}$, and the Lamb-Dicke parameter η which characterizes the ratio of the width of axis within which the ion vibrates in the trap to the wavelength of the driving radiation field. By considering the dynamics in the interaction picture with respect to $\mathcal{H}_s + \mathcal{H}_p$ the system Hamiltonian reads

$$\mathcal{H}_I = (\hbar/2)\Omega\sigma_+ \exp[i\eta(ae^{-i\nu t} + a^\dagger e^{i\nu t})]e^{-i\delta t} + \text{H.c.}, \tag{4.3}$$

where the detuning $\delta = \omega - \omega_{eg}$ is the difference between the driving and the resonance frequencies. In the Lamb-Dicke regime [41], where the ion's extension of vibration is negligible compared with the wavelength of the

driving radiation field,

$$\eta \ll 1, \tag{4.4}$$

the Hamiltonian in Eq.(4.3) can be expanded in terms of the coefficient η,

$$\mathcal{H}_I \approx (\hbar/2)\Omega\sigma_+\big(1 + i\eta(ae^{-i\nu t} + a^\dagger e^{i\nu t})\big)e^{-i\delta t} + \text{H.c.}. \tag{4.5}$$

Three cases of radiation detuning $\delta = 0, \pm\nu$ are of particular interest;
carrier resonance ($\delta = 0$) - by applying the second rotating wave approximation the Hamiltonian that generates the carrier transition $|g\rangle \leftrightarrow |e\rangle$ reads

$$\mathcal{H}_{car} = (\hbar/2)\Omega\sigma_x$$

blue-sideband resonance ($\delta = \nu$) - by applying the second rotating wave approximation the Hamiltonian that generates the blue-sideband transition $|g\rangle|n\rangle \leftrightarrow |e\rangle|n+1\rangle$ reads

$$\mathcal{H}_{bsb} = (\hbar/2)\eta\Omega(a\sigma_- + a^\dagger\sigma_+) \tag{4.6}$$

red-sideband resonance ($\delta = -\nu$) - by applying the second rotating wave approximation the Hamiltonian that generates the red-sideband transition $|g\rangle|n\rangle \leftrightarrow |e\rangle|n-1\rangle$ reads

$$\mathcal{H}_{rsb} = (\hbar/2)\eta\Omega(a\sigma_+ + a^\dagger\sigma_-). \tag{4.7}$$

As one can see in the case of carrier resonance the vibration of the ion is not affected, whereas in the case of blue/red-sideband resonance the internal and the external degrees of freedom of the ion get correlated. Three cases of transitions are illustrated in Fig.(4.2).

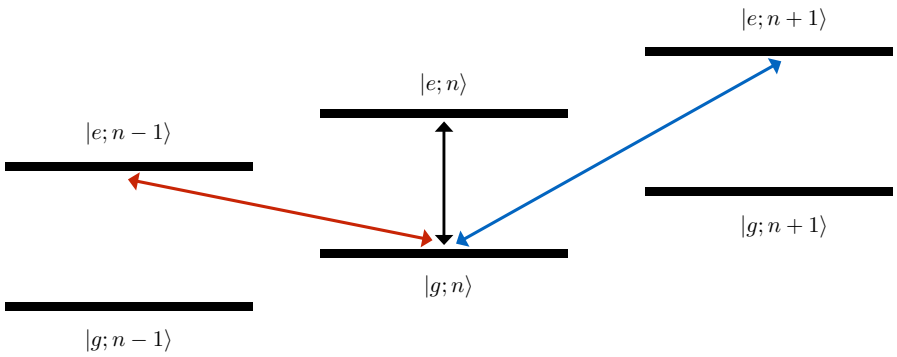

Figure 4.2: Scheme for carrier (black arrow), blue sideband (blue arrow), and red sideband transitions (red arrow).

4.2 Entangling Gates

It has been shown that any arbitrary unitary process can be simulated to an arbitrary accuracy by constructing a network of single-qubit and two-qubit gates [42] - a set of universal quantum gates [43]. Two-qubit gates provide the mechanism to drive the qubits into an entangled state. In the trapped ion implementation of quantum computation, however, the qubits - the set of two-level internal degrees of freedom - do not experience a *direct* interaction among each other, and therefore, the spin states of the ions are to a high degree of accuracy insensitive to one another. The interaction between these spin states can be mediated by their collective mode of vibration - the bus mode. Since correlating the spin state and the collective motional state of the ions is possible via blue/red-sideband resonance radiation, one can induce an *indirect* interaction between the spin states of the ions as depicted in Fig.(4.3).

One of the fundamental operations in information processing is *controlled unitaries*. In quantum computation a typical controlled unitary is

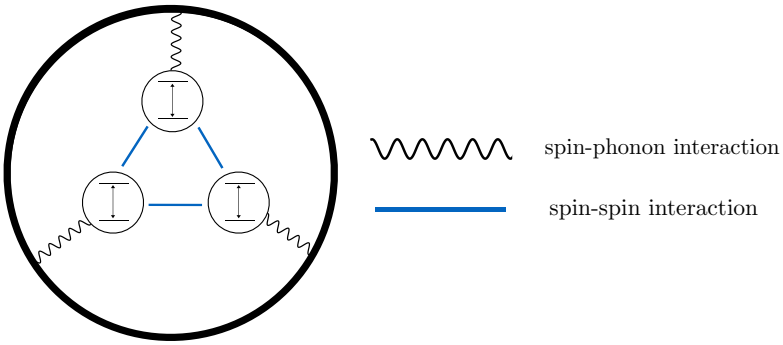

Figure 4.3: Scheme for the induced spin-spin interaction among a set of trapped ions through their direct interaction with their collective vibrational mode -phonon mode.

the controlled-NOT(CNOT) operation, a quantum gate consisting of two qubits, control qubit and target qubit, respectively. The CNOT gate flips the state of the target qubit if and only if the state if the control qubit is $|1\rangle$,

$$|\epsilon_1\rangle|\epsilon_2\rangle \rightarrow |\epsilon_1\rangle|\epsilon_1 \oplus \epsilon_2\rangle, \tag{4.8}$$

where $|\epsilon_1\rangle, |\epsilon_2\rangle$ represent the computational basis, and $\oplus$ denotes the addition modulo 2.

4.3 Cirac-Zoller scheme

A CNOT gate can be implemented using a system of trapped ions by applying Cirac-Zoller (CZ) scheme[2, 10]. First, the qubit state of the control ion is mapped on to the bus mode. Second, a controlled phase gate oper-

ation is performed on the target qubit conditioned on the state of the bus mode. Finally the state of the bus mode is mapped back on the state of the control qubit.

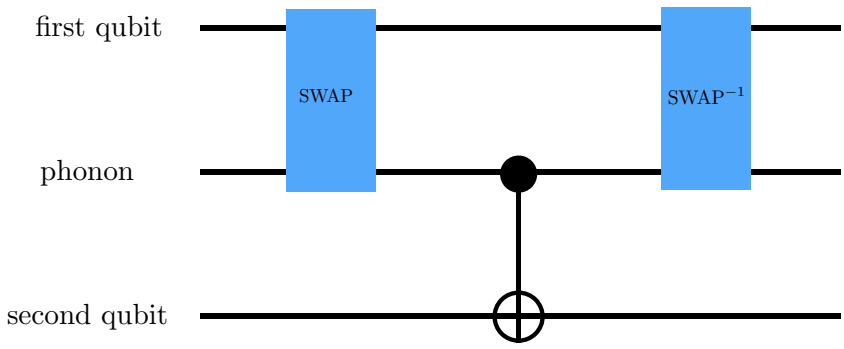

Figure 4.4: Diagram of the CZ gate - $SWAP = R_1^+(\pi, 0)$, $SWAP^{-1} = R_1^+(\pi, \pi)$, and the CNOT operation representing the composite pulse sequence, $R_2(\pi/2, 0)R_2^+(\pi, 0)R_2^+(\pi/\sqrt{2}, \pi/2)R_2^+(\pi, 0)R_2^+(\pi/\sqrt{2}, \pi/2)R_2(\pi/2, \pi)$.

The CZ gate can be implemented in terms of the carrier transition and the blue-sideband transition denoted by $R(\theta, \phi)$ and $R^+(\theta, \phi)$ respectively. Here θ denotes the Rabi angle and ϕ denotes the pulse phase as following

$$\begin{aligned} R(\theta, \phi) &= \exp[-i\frac{\theta}{2}(\sigma_- e^{i\phi} + \sigma_+ e^{-i\phi})] \\ R^+(\theta, \phi) &= \exp[-i\frac{\theta}{2}(a\sigma_- e^{i\phi} + a^\dagger \sigma_+ e^{-i\phi})]. \end{aligned} \tag{4.9}$$

First step of the gate [10] incorporates a blue-sideband resonance radiation field with a pulse duration of π, $R_1^+(\pi, 0)$. The π-pulse applied to the blue sideband of the first ion, maps the ion's spin state to a corresponding phonon state of the bus mode. The phonon state itself forms a qubit with $|n = 0, 1\rangle$ representing the logical state $|1, 0\rangle$. Now that the quantum

information of the first qubit is stored in the phonon state, the second ion is addressed and a CNOT gate operation between this ion and bus mode can be implemented. This is done using composite pulse techniques by constructing the pulse sequence

$$R_2^+(\pi,0)R_2^+(\pi/\sqrt{2},\pi/2)R_2^+(\pi,0)R_2^+(\pi/\sqrt{2},\pi/2).$$

This pulse sequence encodes a single-ion phase gate, and can be represented in terms of the following matrix

$$\begin{bmatrix} -1 & 0 & 0 & 0 \\ 0 & -1 & 0 & 0 \\ 0 & 0 & -1 & 0 \\ 0 & 0 & 0 & 1 \end{bmatrix}$$

with the basis being $\{|\epsilon_2 = 0; n = 1\rangle, |\epsilon_2 = 1; n = 1\rangle, |\epsilon_2 = 0; n = 0\rangle, |\epsilon_2 = 1; n = 0\rangle\}$. By enclosing this operation (controlled phase gate) on the left and the right side, with two carrier $\pi/2$-pulses, $R_2(\pi/2, 0)$ and $R_2(\pi/2, \pi)$ respectively, one obtains a single-ion CNOT gate.

The third step consists of another π-pulse on the blue sideband of the first ion, $R_1^+(\pi, \pi)$, in order to bring back the qubit and the phonon to their original states.(see Fig.(4.4)).

4.4 Mølmer-Sørensen Scheme

An alternative way to realise entangling quantum gates based on system of trapped ions is the Mølmer-Sørensen(MS) scheme [3] which involves the collective driving via the radiation fields rather than the individual addressing of the ions which was proposed in the CZ scheme. As we will see in the following, an important aspect of the MS scheme is that the gate operation is insensitive to the collective vibrational state of the ions, that is, the gate can be carried out even if the bus mode of the ions is not in

its ground state. In the MS scheme a string of trapped ions is being illuminated by two control radiation fields that are slightly detuned from the blue-sideband and the red-sideband resonance of the bus mode respectively.

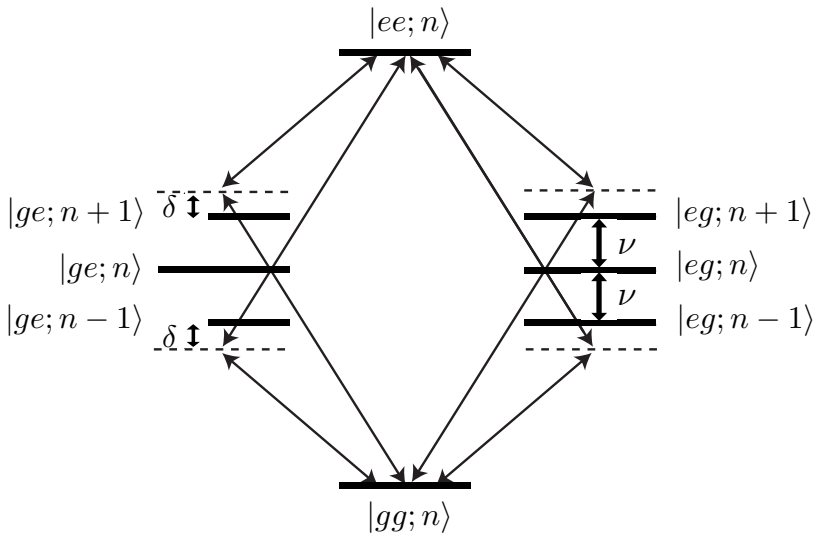

Figure 4.5: Level scheme of two-qubit MS gate; ions sharing a collective vibrational mode are illuminated by two laser radiation fields that are symmetrically detuned from the sideband levels. The radiation field couples qubit states $|gg\rangle \leftrightarrow |ee\rangle$ through the four interfering transition paths.

In the MS scheme the intermediate states with different vibrational levels are essential in the performance of the gate, since their presence during the gate operation is crucial in generating spin-phonon coupling, and thus mapping the information stored in the qubit into the vibrational degree of freedom (phonon) which is shared by all the other qubits as we will describe in mathematical terms later. Furthermore, by having these intermediate states negligibly occupied, the population gets effectively shared

amongst the $|gg;n\rangle$ and $|ee;n\rangle$ states only *e.g.*

$$|\psi\rangle = c_1|gg;n\rangle + c_2|ee;n\rangle. \tag{4.10}$$

Moreover, the sensitivity of the gate to the state of the bus mode diminishes as the transition path through different vibrational states interfere destructively, and as we mentioned earlier this permits the gate to be carried out even if the collective vibrational mode of the ions is not in its ground state. The MS Hamiltonian encoding the mathematics of the gate dynamics can be constructed by the addition of the Hamiltonians $H^{(-)}(t)$ and $H^{(+)}(t)$ corresponding to the red-sideband and the blue-sideband off-resonant transitions respectively obtained in Eq.(4.7, 4.6) with the detuning δ from the sideband resonances as has been shown in the Fig.(4.5)

$$\begin{aligned}
\mathcal{H}_{MS}(t) &= H^{(-)}(t) + H^{(+)}(t) \\
&= (\hbar/2)\eta\Omega\big(a\mathcal{S}_+e^{-i\delta t} + a^\dagger\mathcal{S}_-e^{i\delta t} + a\mathcal{S}_-e^{-i\delta t} + a^\dagger\mathcal{S}_+e^{i\delta t}\big) \\
&= (\hbar/2)\eta\Omega\big(ae^{-i\delta t} + a^\dagger e^{i\delta t}\big)\mathcal{S}_x,
\end{aligned} \tag{4.11}$$

where $\mathcal{S}_\pm = \Sigma_{j=1}^N \sigma_\pm^{(j)}$ and $\mathcal{S}_x = \Sigma_{j=1}^N \sigma_x^{(j)}$ are the collective spin-ladder and spin-flip operator with N being the number of the ions. The unitary dynamics induced by this Hamiltonian can be generated by utilising the methodology of series expansions namely, Magnus series which was introduced in the previous chapter as following

$$\mathcal{U}_{MS}(t) = e^{\mathfrak{M}^{(1)}(t)+\mathfrak{M}^{(2)}(t)+\ldots} \tag{4.12}$$

with

$$\mathfrak{M}^{(1)}(t) = \int_0^t dt'(-i\mathcal{H}_{MS}(t')) \tag{4.13}$$

$$\mathfrak{M}^{(2)}(t) = 1/2\int_0^t dt'[-i\mathcal{H}_{MS}(t'), \mathfrak{M}^{(1)}(t')] \tag{4.14}$$

$$\mathfrak{M}^{(j)}(t) = 0 \qquad j > 2. \tag{4.15}$$

Since all the higher order terms in the Magnus series vanish as a direct consequence of the commutation relation of the phonon operators $[a, a^\dagger] = 1$, one can obtain the exact dynamics. By constructing the terms in the series one can clearly understand the mechanism through which the entanglement between the qubits is achieved,

$$\mathfrak{M}^{(1)}(t) = -i(\alpha(t)a + \alpha^*(t)a^\dagger)\mathcal{S}_x \tag{4.16}$$

$$\mathfrak{M}^{(2)}(t) = i\Phi(t)\mathcal{S}_x^2 \tag{4.17}$$

where

$$\alpha(t) = \eta\Omega \int_0^t dt' e^{i\delta t'} \quad \text{and} \tag{4.18}$$

$$\Phi(t) = \eta^2\Omega^2 \int_0^t dt' \int_0^{t'} dt'' \sin(\delta(t' - t'')). \tag{4.19}$$

The first order term encodes the transient entanglement of the spin degrees of freedom with the bus mode - coupling to sideband resonances - since it couples the spin operator with phonon operators, whereas the second order term generates the entanglement process - the functionality of the gate. In order to achieve entanglement through this scheme, that is to simulate the spin-spin coupling, one needs to suppress the first order term in the series $\mathfrak{M}^{(1)}$ which would be equivalent to the spin-phonon disentanglement after the gate duration. One can see that by setting the gate-time to be $t_g = 2\pi/\delta$ the propagator $\mathcal{U}_{MS}$ reads

$$\mathcal{U}_{MS}(t_g) = e^{\Phi(t_g)\mathcal{S}_x^2}, \quad \text{with} \quad \Phi(t_g) = -\hbar\frac{(\eta\Omega)^2}{\delta}\frac{2\pi}{\delta}. \tag{4.20}$$

So by controlling the relation between Ω and δ any entangled stated of the qubits can be achieved, for instance by setting $\Omega/\delta = 1/4$, one obtains an operation inducing a maximally entangled state *e.g.* $\mathcal{U}_{MS} = e^{-i\frac{\pi}{8}\mathcal{S}_x^2}$.

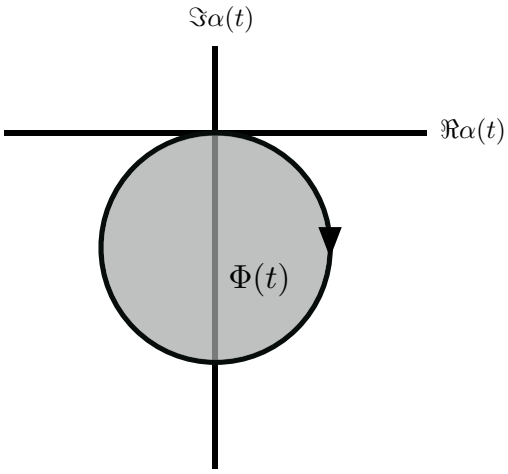

Figure 4.6: Phase-space representation of the MS gate; excursion of the trajectory represents the displacement of the phonon mode, and the area swept by the trajectory represents the phase gate $\Phi(t)$.

Displacement in phase-space

The entangling gate operation

$$\mathcal{U}_{MS}(t) = \exp\Big(-i\big(\alpha(t)a + \alpha^*(t)a^\dagger\big)\mathcal{S}_x - \Phi(t)\mathcal{S}_x^2\big)\Big), \tag{4.21}$$

is based on a displacement of the bus mode in phase space conditioned on the state of the qubit degrees of freedom. By rewriting Eq.(4.21) in the basis $\{x, p\}$ defined as $x = a + a^\dagger$ and $p = i(a - a^\dagger)$, one can obtain the phase-space representation of the MS gate dynamics as

$$\mathcal{U}_{MS} = \exp\Big(-i\big((\Re\alpha(t)x + \Im\alpha(t)p)\mathcal{S}_x - \Phi(t)\mathcal{S}_x^2\big)\Big). \tag{4.22}$$

As one would expect, according to Eq.(4.22) the spin-phonon coupling during the gate operation can be represented as closed circular trajectories in the phase space spanned by the real and imaginary part of the function

$\alpha(t)$. Furthermore, the area swept by the trajectory is equal to the gate phase $\Phi(t)$ as depicted in Fig.(4.6).

Part II

Analysis of Driven Systems

Chapter 5

Approximate Dynamics

5.1 Effective Dynamics

As we discussed in chapter 2, in order to approximate the behaviour of an open quantum system with a time-dependent generator, one can resort to series expansion methodology. Here we will construct an expansion obtained using the Magnus series,

$$\mathcal{E}(t) = e^{\mathfrak{L}(t)} = e^{\mathfrak{L}^{(1)}(t)+\mathfrak{L}^{(2)}(t)+\cdots}, \tag{5.1}$$

where the terms in the exponent are given in Eq.(3.10). Assuming periodic driving with period T, the generator $\mathfrak{L}(t)$ defines the effective generator $\mathfrak{L}_{\text{eff}} = \mathfrak{L}(T)/T$, which satisfies

$$\mathcal{E}(nT) = e^{\mathfrak{L}_{\text{eff}} nT} \tag{5.2}$$

for all integer n. Under a stroboscopic perspective in which the system is monitored at multiples of driving periods only, the effective generator $\mathfrak{L}_{\text{eff}}$ and $\mathcal{L}(t)$ induce the same dynamics, so that a system with the time-dependent generator $\mathcal{L}(t)$ simulates the dynamics induced by $\mathfrak{L}_{\text{eff}}$.

The main problem is that the partial sum of the Magnus series $\mathfrak{L}_n(T)/T$ generates a map which is not necessarily completely positive, and therefore, it does not respect the algebraic structure of the open system dynamics. As we discussed in Part I, in order to simulate the behaviour of an open quantum system one needs to be able to manipulate and control the behaviour of the underlying generator; that is the simulation of the effective behaviour of any open quantum systems can not be achieved without having access to a valid effective generator. As we will discuss in this chapter, our goal is to design a correction scheme by which the partial sum $\mathfrak{L}_n(T)/T$ can be modified and replaced with a corrected finite series $\tilde{\mathfrak{L}}_n(T)/T$ which does indeed induce a completely positive dynamics.

As we discussed in chapter 3, an essential aspect of the series expansion of the generator instead of the propagator for closed systems is that it yields a unitary, approximate propagator in any order of approximation. Due to the exponential function, which can be mathematically represented in terms of an *infinite* series, the propagator with an n-th order generator contains terms of higher than n-th order, and it is exactly those terms that make sure that the fundamental property of unitarity is preserved. In a similar fashion, in order to preserve the fundamental property of complete positivity, we will consider the incorporation of suitably chosen higher order terms in the construction of the generator so that a valid approximate dynamics can be induced. As one would expect, incorporation of fundamental principles such as unitarity or complete positivity would systematically help to improve the accuracy of the approximation.

Although the solution of the master equation with a time-dependent generator encodes the irreversible dynamics of an open quantum system, a completely positive map, it can not necessarily be represented in terms of an exponential function of the form

$$\mathcal{E}(t) = e^{\mathfrak{L}(t)}, \tag{5.3}$$

where $\mathfrak{L}(t)$ is of the Lindblad form [44]; that is to say not every completely positive map does not necessarily represent a Markovian dynamics. Considering an infinitesimal dynamics, the celebrated Lindblad form [25]

$$\mathcal{L}[\circ] = -i[\mathcal{H}, \circ] + \sum_{ij} [\mathbb{C}]_{ij} (E_i \circ E_j^\dagger - \frac{1}{2}\{E_j^\dagger E_i, \circ\}) \tag{5.4}$$

with a positive-semidefinite, Hermitian coefficient matrix $\mathbb{C}$ characterizes all valid generators, in general however, the prescription of generators of completely positive maps is a largely open question, and the Lindblad form is only a sufficient, but not a necessary condition [44, 45].

The series expansion [33–35] at finite order n provides an approximate generator $\mathfrak{L}_n$ of the form of Eq.(5.4), that under stroboscopic perspective permits to read off an effective Hamiltonian $\mathcal{H}_n$ and an effective coefficient matrix $\mathcal{C}_n$,

$$\begin{aligned} \mathfrak{L}_n(T)/T[\circ] &= -i[\mathcal{H}_n, \circ] + \sum_{i,j=1}^{N^2-1} [\mathcal{C}_n]_{ij} (E_i \circ E_j^\dagger - \frac{1}{2}\{E_j^\dagger E_i, \circ\}) \quad \text{with} \\ \mathcal{H}_n &= \sum_{j=0}^{n} \frac{\mathcal{H}^{(j)}}{\omega^j} \\ \mathcal{C}_n &= \sum_{j=0}^{n} \frac{\mathcal{C}^{(j)}}{\omega^j}. \end{aligned} \tag{5.5}$$

Here ω is the fundamental frequency of the driving field, $\omega = 2\pi/T$, and as one can see, under stroboscopic observation it can be considered as the perturbation parameter in the approximation, and this ensures the convergence of the series expansion. In other words, by monitoring the system dynamics at integer-multiples of the period, and in the regime where the driving frequency is larger than the Rabi frequency,the convergence of the Magnus series is ensured. As the ratio of the driving amplitude to the driving frequency grows, that is one approaches the regime of fast driving, the difference between the exact and the effective behaviour diminishes.

Moreover, the contribution of the lower order terms in the series expansion become more dominant as the norm of the higher order terms tend to zero, and this ensures the convergence of the series expansion.

The central flaw is, that $\mathcal{C}_n$ is not necessarily a positive semidefinite matrix, so that complete positivity of the induced dynamics is not ensured. As we mentioned in Chapter 3, the series expansion is valid up to the order of truncation n, so that modifications of the series at the higher orders $j > n$ are permitted from the mathematical perspective. Adding a term $\sum_{j=n+1}^{n'} \mathcal{C}^{(j)}\omega^{-j}$ with suitably chosen matrices $\mathcal{C}^{(j)}$ $(j > n)$ might result in a positive-semidefinite matrix $\tilde{\mathcal{C}}_n = \sum_{j=0}^{n'} \mathcal{C}^{(j)}\omega^{-j}$, and the generator $\tilde{\mathfrak{L}}_n(T)/T$ defined in terms of $\mathcal{H}_n$ and $\tilde{\mathcal{C}}_n$

$$\mathfrak{L}_n(T)/T[\circ] = -i[\mathcal{H}_n, \circ] + \sum_{i,j=1}^{N^2-1} [\tilde{\mathcal{C}}_n]_{ij}(E_i \circ E_j^\dagger - \frac{1}{2}\{E_j^\dagger E_i, \circ\})$$

would be a valid generator of open quantum system dynamics.

Since positivity of a matrix in general is a concept of mathematical inequality, there is no unique choice for the matrices $\mathcal{C}^{(j)}$ $(j > n)$ which leaves substantial ambiguity in the construction of a valid generator. In the following we will present the methods which we have investigated in the construction of positive-semidefinite matrices and will discuss their limitation in obtaining such coefficient matrices.

5.2 Correction Methods

factorisation method

In the first method the non-positive coefficient matrix $\sum_{j=0}^{n} \mathcal{C}^{(j)}\omega^{-j}$ gets replaced by a positive-semidefinite matrix according to the following pro-

cedure

$$\sum_{j=0}^{n} \mathcal{C}^{(j)}\omega^{-j} \longrightarrow \sum_{j,k=0}^{n} \eta_j \eta_k^{\dagger}/\omega^{-(j+k)} \tag{5.6}$$

which induces a set of one-to-one recursive equations with non-unique solutions

$$\begin{aligned} \mathcal{C}^{(0)} &= \eta_0\eta_0^{\dagger} \\ \mathcal{C}^{(1)} &= \eta_0\eta_1^{\dagger} + \eta_1\eta_0^{\dagger} \\ &\vdots \\ \mathcal{C}^{(n)} &= \sum_{j=0}^{n} \eta_j\eta_{n-j}^{\dagger}. \end{aligned}$$

From this we can solve for the matrix η_j for $j > 0$ and realise the matrix $\sum_{j,k}^{n} \eta_j\eta_k^{\dagger}/\omega^{-(j+k)}$ with $j + k > n$, which appears on the right-hand side of the Eq.(5.6) acting as a correction to the series expansion obtained using Magnus series. Alternatively, $\sum_{j,k}^{n} \eta_j\eta_k^{\dagger}/\omega^{-(j+k)}$ with $j + k > n$ can be viewed as the term which captures the impact of the higher order terms that have been neglected because of the truncation. In order to see why this method is problematic, let us consider the series expansion truncated at the first order

$$\mathcal{C}^{(0)} + \mathcal{C}^{(1)}/\omega \longrightarrow (\eta_0 + \eta_1/\omega)(\eta_0 + \eta_1/\omega)^{\dagger} \tag{5.7}$$

from which one can deduce the following set of equations

$$\begin{aligned} \mathcal{C}^{(0)} = \eta_0\eta_0^{\dagger} \quad &\Rightarrow \quad \eta_0 = (\mathcal{C}^{(0)})^{\frac{1}{2}}U \\ \mathcal{C}^{(1)} = \eta_0\eta_1^{\dagger} + \eta_1\eta_0^{\dagger} \quad &\Rightarrow \quad \eta_1 = (\frac{\mathcal{C}^{(1)}}{2})\eta_0^{-1} + i\zeta \\ \text{correction} \quad &\equiv \quad \eta_1\eta_1^{\dagger}/\omega^2. \end{aligned} \tag{5.8}$$

Here U and ζ are unitary and self-adjoint matrices respectively, which indicates that the solution for η_0 and η_1 are not unique. On the other hand

these matrices can be considered as a set of additional variables based on which the correction term can be chosen such that minimal values of $\| \sum_j^n \mathcal{C}^{(j)}\omega^{-j} - \sum_{j,k=0}^n \eta_j\eta_k^\dagger/\omega^{-(j+k)} \|_2$ is obtained; that is by applying the least amount of modification, the positive-semidefinite matrix can be deduced. Also here one can see that correction to the series is essentially the addition of terms of higher orders in the powers of $1/\omega$. The central problem with this correction method however, is that the matrix η_1 can not be mathematically defined if the matrix η_0 is not invertible as one can see from Eq.(5.8), and this problem can not be lifted by incorporation of any unitary matrix in the construction of η_0 since $\det(\eta_0 U) = \pm\det(\eta_0)$. Invertibility of η_0 is directly related to the invertibility of the coefficient matrix $\mathcal{C}_0$, which is not necessarily satisfied.

mutation method

In this method, we study the positivity of the coefficient matrix by examining the determinant of a class of its sub-matrices called *principal minors*. The minor M_{ij} of a square matrix is the determinant of its sub-matrix formed by removing its i^{th} row and j^{th} column multiplied by the co-factor $(-1)^{i+j}$

$$M_{ij} = (-1)^{i+j}\det\begin{bmatrix} a_{11} & a_{12} & \cdots & a_{1j} & \cdots & a_{1n} \\ a_{21} & a_{22} & \cdots & a_{2j} & \cdots & a_{2n} \\ \vdots & \vdots & \ddots & \vdots & \ddots & \vdots \\ a_{i1} & a_{i2} & \cdots & a_{ij} & \cdots & a_{in} \\ \vdots & \vdots & \ddots & \vdots & \ddots & \vdots \\ a_{n1} & a_{n2} & \cdots & a_{nj} & \cdots & a_{nn} \end{bmatrix}$$

In order to examine whether a self-adjoint matrix is positive-semidefinite there exist a criterion [46] which states that a self-adjoint matrix is positive-

semidefinite iff all of its principal minors are non-negative; here principal minor refers to the minor M_{ij} where $i = j$. In other words, the method is based on forming these sub-matrices and modifying their elements by adding terms of higher orders in powers of $1/\omega$ so that determinant of the principle minor become non-negative numbers. The problem with this method can be understood in terms of a simple example; let us assume that the coefficient matrix truncated at the second order reads

$$\mathcal{C}_2 = \begin{bmatrix} 0 & \frac{1}{\omega} \\ \frac{1}{\omega} & 1 + \frac{1}{\omega^2} \end{bmatrix}.$$

Here one needs to add a term of order $\mathcal{O}(\omega^{-3})$ to the elements of the matrix in order to make the determinant a non-negative number. In order to see why this is not possible, let us include a correction matrix incorporating all the higher order terms in $1/\omega$ as following

$$\tilde{\mathcal{C}}_2 = \mathcal{C}_2 + \begin{bmatrix} \alpha & \beta \\ \beta^* & \delta \end{bmatrix}, \tag{5.9}$$

where $\{\alpha, \beta, \delta\} \sim \mathcal{O}(\omega^{-3})$. The determinant of $\tilde{\mathcal{C}}_2$ reads

$$\begin{aligned} \det[\tilde{\mathcal{C}}_2] &= \alpha(1 + \frac{1}{\omega^2} + \delta) - \frac{1}{\omega}(\beta + \beta^*) - \beta\beta^* - \frac{1}{\omega^2} \\ \det[\tilde{\mathcal{C}}_2] &\sim -\frac{1}{\omega^2} + \mathcal{O}(\omega^{-3}) \not\geq 0. \end{aligned} \tag{5.10}$$

In other words, the determinant can not be non-negative for all values of ω. Alternatively, the correction matrix which sets the determinant to zero reads

$$\mathcal{C}_{correction} = \begin{bmatrix} \frac{1}{1+\omega^2} & 0 \\ 0 & 0 \end{bmatrix},$$

which simply can not be constructed from the higher order terms $\mathcal{O}(\omega^{-3})$. There are examples for which the correction scheme based on matrix mu-

tation can be applied; in general however, it fails to stand as a generic and system-independent framework. Such correction framework in principle can be obtained through the following method.

perturbative method

In this method, we address the eigenvalues of the coefficient matrix obtained using perturbation theory and modify them by incorporating higher-order terms in the powers of the perturbation parameter $1/\omega$. Typically it is possible to diagonalise the coefficient matrix $\mathcal{C}_n$ using the methodology of perturbation theory in powers of $1/\omega$. The corresponding eigenvalues $\{\lambda_i\}$ are then approximated as

$$\lambda_i^{(n)} = \sum_{j=j_0}^{n} \mu_{ij}\omega^{-j} \tag{5.11}$$

with the leading non-vanishing contribution labelled by j_0. Our aim is to replace $\{\lambda_i\}$ with a set of eigenvalues $\{\tilde{\lambda}_i\}$ satisfying the following conditions

$$\begin{aligned} \tilde{\lambda}_i^{(n)} &> 0 && (1) \\ \lambda_i^{(n)} - \tilde{\lambda}_i^{(n)} &\sim \mathcal{O}(\frac{1}{\omega^{n+1}}) && (2) \end{aligned}$$

for all indices i and any given order n. That is, the eigenvalues of the original and the corrected matrices should coincide up to the order of the approximation in the Magnus series, and furthermore, the eigenvalues of the corrected matrix should be non-negative. Conditions (1) and (2) imply the

two following equalities

$$\begin{aligned} \tilde{\lambda}_i^{(n)} &= \sum_{j,k=j_0}^{m} \nu_{ij}\nu_{ik}\omega^{-(j+k)}, \\ \sum_{j=j_0}^{n} \mu_{ij}\omega^{-j} &= \sum_{j,k=j_0}^{m} \nu_{ij}\nu_{ik}\omega^{-(j+k)} \quad \text{for} \quad j+k \leq n. \end{aligned} \tag{5.12}$$

From this the following set of equations with unique recursive solutions can be obtained

$$\mu_{in} = \sum_{j=j_0}^{n} (\nu_{ij}\nu_{i,n-j+j_0})\omega^{-j_0}. \tag{5.13}$$

Higher order terms can uniquely be calculated by imposing the condition $m = n$. Therefore, the variables ν can uniquely be computed as

$$2\nu_{in} = \frac{1}{\nu_{ij_0}}(\omega^{j_0}\mu_{in} - \sum_{j=j_0+1}^{n-1} \nu_{ij}\nu_{ij'}) \tag{5.14}$$

where $j' = n + j_0 - j$ and $\nu_{ij_0} = \sqrt{\mu_{ij_0}}\omega^{j_0}$. As one can see, this method is applicable iff the leading contribution μ_{ij_0} is non-negative. Following this strategy, one can define a positive semidefinite matrix

$$\tilde{\mathcal{C}}_n = \sum_i \tilde{\lambda}_i^{(n)} \Phi_i^{(n)} (\Phi_i^{(n)})^\dagger \tag{5.15}$$

in terms of the perturbatively obtained eigenvectors $\Phi_i^{(n)}$ of $\mathcal{C}_n$. Since the difference between $\lambda_i^{(n)}$ and $\tilde{\lambda}_i^{(n)}$ is of at least $n+1^{st}$ order, the $\tilde{\mathcal{C}}_n$ is consistent with the order n of expansion, and a generator $\tilde{\mathcal{L}}_n$ defined via Eq.(5.4) with the coefficient matrix $\tilde{\mathcal{C}}_n$ does indeed induce completely positive dynamics.

By diagonalising the effective generator, we obtain

$$\tilde{\mathfrak{L}}_n(T)/T[\circ] = -i[\mathcal{H}_n, \circ] + \sum_j \tilde{\Gamma}_j^{(n)} \mathcal{D}_{\mathcal{P}_j^{(n)}}[\circ] \tag{5.16}$$

in terms of effective Lindblad operators $\mathcal{P}_j^{(n)}$ and associated rates $\tilde{\gamma}_j^{(n)}$. With this, one obtains a physical interpretation of the dynamics of the driven dissipative system, in terms of effective decoherence processes of a static system described by the Lindblad operators $\mathcal{P}_j^{(n)}$ and decoherence rates $\tilde{\Gamma}_j^{(n)}$. Therefore, by preserving the property of complete positivity, the proposed eigenvalue modification procedure can be considered as a correction scheme which identifies the approximate but valid effective dissipative processes and their corresponding rates in the treatment of open quantum system dynamics.

In the following we will show with several explicit examples that the approximate generator often can be extended to be of Lindblad form consistently with the given order of expansion. By comparing the dynamics induced by theses corrected generators $\tilde{\mathfrak{L}}_n$ with the numerically obtained exact solutions of driven open quantum systems we will demonstrate that in addition to completely positive dynamics the corrected generators $\tilde{\mathfrak{L}}_n$ also provide a substantially better approximation of the exact dynamics than their counterpart $\mathfrak{L}_n$.

5.3 Two-Level System

Let us begin with the driven two-level system whose Hamiltonian can be written as

$$H_{tl}(t) = \frac{\omega_0}{2}\sigma_z + (\Omega_s \sin(\omega t) + \Omega_c \cos(\omega t))\sigma_x \tag{5.17}$$

in terms of the Pauli matrices $\{\sigma_i\}$, the resonance frequency ω_0 of the bare system, and the driving amplitudes for *sine* and *cosine* driving. In the presence of dephasing with rate γ which itself may depend on the driving, the time-dependent generator $\mathcal{L}_{tl}(t)$ reads

$$\mathcal{L}_{tl}(t)[\circ] = -i[H_{tl}(t), \circ] + \gamma \mathcal{D}_{\sigma_z}[\circ]. \tag{5.18}$$

By constructing the series expansion as explained in detail in Sec. A.1

the resulting effective Hamiltonian reads

$$\frac{\mathcal{H}_n}{\omega_0} = \left(\frac{1}{2} - \frac{\Omega_c^2 + 3\Omega_s^2}{2\omega^2}\right)\sigma_z + \frac{\Omega_s}{\omega}\sigma_y + \Omega_c\frac{4\gamma^2 - \omega_0^2}{\omega_0\omega^2}\sigma_x + ... \tag{5.19}$$

In lowest and first order approximation the effective Hamiltonians coincide with that of the coherent system [33] with no influence of dephasing; by including the higher order terms however, the reversible dynamics is affected by the dephasing factor as can be seen from the Eq.(5.19). But in second order, the effective Hamiltonian is actually influenced by the presence of dephasing. The main impact of dephasing is, however, encoded in the coefficient matrix $\mathcal{C}_n$ which reads

$$\mathcal{C}_n = \begin{bmatrix} 0 & 0 & 0 \\ 0 & 0 & 0 \\ 0 & 0 & \gamma \end{bmatrix} + \frac{1}{\omega}\begin{bmatrix} 0 & 0 & 0 \\ 0 & 0 & \alpha \\ 0 & \alpha & 0 \end{bmatrix} + \frac{1}{\omega^2}\begin{bmatrix} 0 & 0 & \beta \\ 0 & \xi & 0 \\ \beta & 0 & -\xi \end{bmatrix} + \mathcal{O}(\omega^{-3})$$

with $\alpha = 2\gamma\Omega_s$, $\beta = -4\gamma\omega_0\Omega_c$, $\xi = 2\gamma(\Omega_c^2 + 3\Omega_s^2)$ in the space spanned by the Pauli matrices $\{\sigma_j\}$. At the lowest order of the approximation, $\mathcal{C}_0$ coincides with time-independent coefficient matrix $\mathbb{C}$, which encodes the dissipative rates, and therefore is necessarily positive-semidefinite. In contrast, by including the first order contribution in the series, we obtain the matrix $\mathcal{C}_1$, which is not positive-semidefinite as it comprises negative eigenvalues

$$\begin{aligned} \lambda_1^{(1)} &= \gamma(1 + \alpha^2/\omega^2 + \mathcal{O}(\omega^{-3})), \\ \lambda_2^{(1)} &= 2\gamma(-\alpha^2/\omega^2 + \mathcal{O}(\omega^{-3})), \\ \lambda_3^{(1)} &= 0. \end{aligned} \tag{5.20}$$

Based on the proposed correction scheme, at the given order n, any polynomial modification at the order $\mathcal{O}(\omega^{-(n+1)})$ is permitted from mathematical perspective. Thus, we can simply cut off all the terms of the order $\mathcal{O}(\omega^{-2})$,

and retrieve the following values

$$\begin{aligned}\tilde{\lambda}_1^{(1)} &= \gamma \\ \tilde{\lambda}_2^{(1)} &= 0, \\ \tilde{\lambda}_3^{(1)} &= 0.\end{aligned} \tag{5.21}$$

Together with the corresponding eigenvectors $\{\Phi_j^{(1)}\}$, we construct the following positive-semidefinite matrix

$$\tilde{\mathcal{C}}_1 = \gamma \begin{bmatrix} 0 & 0 & 0 \\ 0 & 4\Omega_s^2/\omega^2 & 2\Omega_s/\omega \\ 0 & 2\Omega_s/\omega & 1 \end{bmatrix}, \tag{5.22}$$

which together with the effective Hamiltonian $\mathcal{H}_1$ defines the valid generator

$$\tilde{\mathfrak{L}}_1(T)/T[\circ] = -i[\frac{\omega_0}{2}(\sigma_z + \frac{2\Omega_s}{\omega}\sigma_y), \circ] + \sum_{ij}[\tilde{\mathcal{C}}_1]_{ij}(\sigma_i \circ \sigma_j - \frac{1}{2}\{\sigma_j\sigma_i, \circ\}). \tag{5.23}$$

We can represent this generator based on the operators $\{\tilde{\sigma}_j\}$ in terms of which the effective Hamiltonian $\mathcal{H}_1$ is diagonal as

$$\tilde{\mathfrak{L}}_1(T)/T[\circ] = -i\left[\frac{\omega_0}{2}\tilde{\sigma}_z, \circ\right] + \gamma\mathcal{D}_{\tilde{\sigma}_z}[\circ]\,. \tag{5.24}$$

The operators $\{\tilde{\sigma}_j\}$ are discussed in detail in Subsec. A.2.1. By comparing this to the generator at the zeroth order, one can clearly see that the only difference between driven and un-driven system is simply a perturbative rotation of the vector space $\{\sigma_j \to \tilde{\sigma}_j\}$ in terms of which the dynamics of the open system is described. The eigenvalues of $\mathcal{C}_2$ including up to second

order contribution read

$$\begin{aligned}\lambda_1^{(2)} &= \gamma - 2\gamma(\Omega_s^2+\Omega_c^2)/\omega^2 + \mathcal{O}(\omega^{-3}),\\ \lambda_2^{(2)} &= 2\gamma(\Omega_s^2+\Omega_c^2)/\omega^2 + \mathcal{O}(\omega^{-3}),\\ \lambda_3^{(2)} &\sim \mathcal{O}(\omega^{-3}).\end{aligned} \tag{5.25}$$

Potentially $\lambda_1^{(2)}$ is not a positive-semidefinite term since, in the regime of strong driving *i.e.* where the Rabi frequency is comparable to the driving frequency, it can adopt negative values. Similarly, we can modify this eigenvalue by introducing higher order terms as

$$\tilde{\lambda}_1^{(2)} = \lambda_1^{(2)} + \gamma\frac{(\Omega_s^2+\Omega_c^2)^2}{\omega^4} = \gamma(1-\frac{\Omega_s^2+\Omega_c^2}{\omega^2})^2,$$

and simply cut off all the terms of the order $\mathcal{O}(\omega^{-3})$ for the other two eigenvalues

$$\begin{aligned}\tilde{\lambda}_2^{(2)} &= 2\gamma(\Omega_s^2+\Omega_c^2)/\omega^2\\ \tilde{\lambda}_3^{(2)} &= 0.\end{aligned} \tag{5.26}$$

Together with the corresponding eigenvectors $\{\Phi_j^{(2)}\}$, this permits to construct a non-negative coefficient matrix $\tilde{\mathcal{C}}_2$, which together with $\mathcal{H}_2$ yields the valid generator $\tilde{\mathfrak{L}}_2$. By representing the effective dynamics in the space $\{\tilde{\sigma}_j\}$, which is perturbatively rotated further up to the order ω^{-2} with respect to $\{\sigma_j\}$, the effective generator $\tilde{\mathfrak{L}}_2$ as explained in detail in Subsec.A.2.1 reads

$$\tilde{\mathfrak{L}}_2(T)/T[\circ] = -i[\frac{\omega_0}{2}(1-\eta)\tilde{\sigma}_z,\circ] + \gamma(1-\eta)^2\mathcal{D}_{\sigma_z'}[\circ] + \gamma\eta\mathcal{D}_{\sigma_y'}[\circ]\,,$$

where $\eta = (\Omega_s^2+\Omega_c^2)/\omega^2$. By comparing the reversible and irreversible parts of the effective dynamics, we can see that the coherent and dephasing processes are represented in terms of two different set of operators $\{\tilde{\sigma}_j\}$ and $\{\sigma_j'\}$ respectively, that are separated by a slight tilt, which is described by

the following unitary transformation

$$\sigma'_k = \sum_l U_{kl}\tilde{\sigma}_l \tag{5.27}$$

with the unitary matrix $U = \exp[-i\frac{\Omega_c}{\omega_0\omega^2}(6\omega_0^2 - 8\gamma^2)\mathscr{G}_5]$ with

$$\mathscr{G}_5 \;=\; \begin{bmatrix} 0 & 0 & -i \\ 0 & 0 & 0 \\ i & 0 & 0 \end{bmatrix}.$$

This is in contrast with the first order approximate dynamics where the transformation $\{\sigma_j \to \tilde{\sigma}_j\}$ was uniform between the reversible and the irreversible parts of the effective generator, and also the dominant dephasing rate $\gamma(1-\eta)^2$ does not coincide with the dephasing rate of the un-driven system. By including higher order terms in the approximation, one can realise several processes which contribute to the construction of the effective behaviour of the driven system to any degree of accuracy.

Up to now, we have provided an analytical description of the approximate dynamics of driven open systems without any reference to the accuracy yielded by these approximations. In the following, we present an assessment of the constructed approximation based on numerically exact simulations.

Fig. 5.1 (a-b) depicts a comparison of the dynamics induced by the effective generators $\mathfrak{L}_n$, in first and second order with the dynamics induced by the corresponding corrected generators $\tilde{\mathfrak{L}}_n$, and with the exact effective dynamics with the following parameters

$$\frac{\Omega_s}{\omega} = \frac{1}{10}, \quad \frac{\Omega_c}{\omega} = \frac{1}{9} \quad \text{and} \quad \frac{\gamma}{\Omega_s} = \frac{1}{8}.$$

The reason for this choice of parameters is as we have mentioned in chapter 3, Magnus expansion tends to high accuracy as the driving frequency becomes larger compared with the Rabi frequency as the series expansion

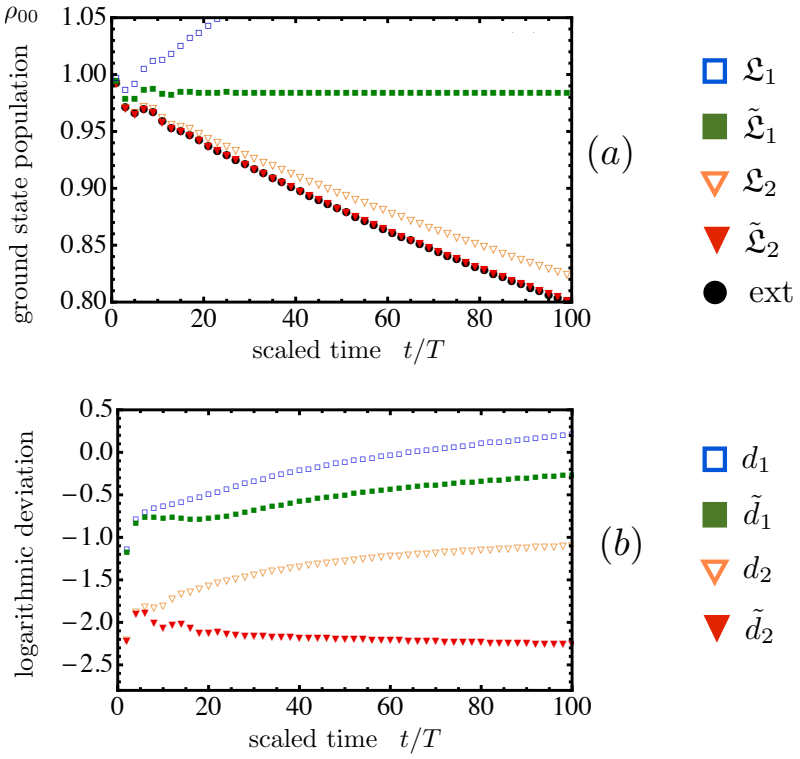

Figure 5.1: Figure (a) depicts the ground state population of a driven, dissipative two-level system as function of time (in multiples of T) for the specific parameters $\Omega_s/\omega = 1/10, \Omega_c/\omega = 1/9$ and $\gamma/\Omega_s = 1/8$. Empty squares (blue) and triangles (orange) depict the approximation in first and second order, and full squares (green) and triangles (red) depict the corresponding completely positive approximations; the exact solution is depicted in full circles (black). Figure (b) depicts the comparison defined in Eq. (5.28) of the propagators in approximation and their extensions that demonstrates the added value of the present completely positive, approximate map.

converges faster; later we present another numerical assessment of the approximation based on a different choice of parameters where the driving and the Rabi frequencies are comparable. Fig.(5.1) - (a) shows the population of the ground state $|0\rangle (= -\sigma_z|0\rangle)$ with $\varrho(0) = |0\rangle\langle 0|$ as initial condition.

At the first order of the approximation, the ground state population decays only for the first few driving periods, after which it suffers a considerable boost, and exceeds the value of 1. Since the dynamics induced by $\mathfrak{L}_1$ is trace-preserving, the population of the excited state must be negative *i.e.* $\langle 1|\varrho|1\rangle < 0$, and therefore, the generated approximation is not completely positive. This defect is suppressed in the dynamics induced by $\tilde{\mathfrak{L}}_1$ which provides a substantial improvement in approximating the exact dynamics; this impact in the accuracy however, does not last long as after a few driving periods, also $\tilde{\mathfrak{L}}_1$ fails to provide a reasonable approximation. At the second order of the approximation, $\mathfrak{L}_2$ generates a largely improved approximation to the exact dynamics; its accuracy however, is not ensured in the entire domain of driving regimes, since in general it does not induce a completely positive dynamics. The corresponding corrected generator $\tilde{\mathfrak{L}}_2$ induces a highly accurate approximation, and this accuracy is maintained comparably for a long driving time scale.

In Fig.(5.1) - (b), we evaluate the approximations based on the induced dynamics rather than the underlying density operators, and demonstrate that this observation is independent of the initial conditions. Inset (b) depicts the logarithmic deviations of the induced dynamics form the exact dynamics in described in terms of

$$d_n = \log ||\mathcal{E}(t) - \mathcal{E}_n(t)||_2 \text{ and } \tilde{d}_n = \log ||\mathcal{E}(t) - \tilde{\mathcal{E}}_n(t)||_2. \tag{5.28}$$

Imposing the condition of complete positivity, generates a significant difference between the deviations $\tilde{d}_n$ and d_n after few driving periods, and furthermore, this contrast extends to an order of magnitude at the second order approximation.

So far we have examined the performance of the approximate dynamics induced by corrected generators $\tilde{\mathfrak{L}}_n$ in the regime of weak/fast driving *i.e.* $\Omega \ll \omega$. We would like to show the remarkable performance of the approximate map in the strong/slow driving regime where the Rabi fre-

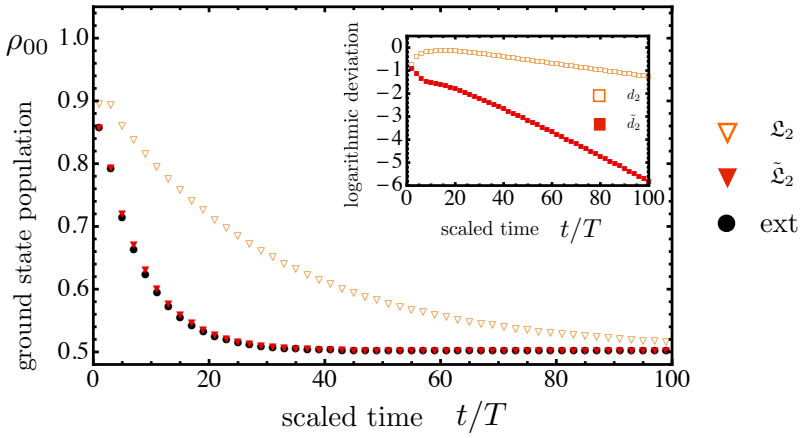

Figure 5.2: Ground state population for a strongly driven dissipative two-level system with the parameters $\Omega_s/\Omega_c = 11/10$ and $\Omega_s/\omega = \gamma/\Omega_s = 1/3$. Despite the failure of the second order approximation (empty triangle (orange)) to approximate the exact dynamics (circle (black)), the corrected expansion in second order (full triangle (red)) induced by $\tilde{\mathfrak{L}}_2$ provides an excellent approximation. The inset shows the logarithmic deviation defined by the (Eq.(5.28)) of the approximate dynamics induced by the original (orange square) and the corrected (red full squares) generators.

quency is not necessarily small compared with the driving frequency *i.e.* $\Omega \lesssim \omega$ as one can see in Fig. 5.2; it depicts the ground state population of a driven two-level system in the extreme regime of strong driving with the parameters $\Omega_s/\Omega_c = 11/10$ and $\Omega_s/\omega = \gamma/\Omega_s = 1/3$. Even in second order, the regular series expansion fails to approximate the actual dynamics, as it is also indicated by the inset that depicts the logarithmic deviation between the actual dynamics an the second order approximation according to Eq. (5.28).

The corrected generator $\tilde{\mathfrak{L}}_2$ on the other hand induces a highly accurate approximation, which underlines the advantage of constructing gen-

erators that induce algebraically valid *e.g.* completely positive dynamics. This may expand the range of analytic problems to which the proposed corrections scheme can be applied. As the inset shows the accuracy of the both original and the corrected approximate dynamics improve with time. This seems to be caused by the strong decoherence regime where the initial state is damped towards a stationary state in a very short time scale within which the induced driven dynamics and also the inaccuracy associated with its approximations are suppressed.

5.4 Harmonic Oscillator

This observed improvement in approximating the dynamics of a dissipative driven system is by no means unique to the two-level system as we examine the behaviour of a driven harmonic oscillator in a dissipative environment. Let us consider a harmonic oscillator with Hamiltonian

$$H_{ho}(t) = \omega_0 \, a^\dagger a + \Omega \sin(\omega t)(a + a^\dagger) \tag{5.29}$$

and Lindblad operator

$$\mathcal{L}_{ho}(t)\circ \;\; = \;\; -i[H_{ho}(t), \circ] + \gamma \mathcal{D}_{\hat{n}}(\circ)$$

where $\{a, a^\dagger\}$ are the creation and annihilation operators with the commutation relation $[a, a^\dagger] = 1$, $\hat{n} = a^\dagger a$ is the phonon-number operator and γ is the dephasing rate. Contrary to the two-level system, harmonic oscillator is not a bounded system, that is, it is described in terms of unbounded operators, and as result of this, the dimension of the effective coefficient matrix is not necessarily finite as it is represented in the space spanned by the set of operators $\{\Pi_{i,j=0}(a^\dagger)^i a^j\}$. Truncating the series expansion at a finite order n however, will result in a coefficient matrix of finite dimension. Here we will consider the terms in the series up to the second order contribution, which leads to a three dimensional space spanned by the set

$\{a, a^\dagger, \hat{n}\}$, in terms of which the effective generator can be represented. The effective Hamiltonian reads

$$\mathcal{H}_n = \omega_0 \hat{n} + \frac{i\Omega\omega_0}{\omega}(a - a^\dagger) + O(\frac{1}{\omega^3}),$$

and the corresponding coefficient matrix reads

$$\mathcal{C}_n = \begin{bmatrix} 0 & 0 & 0 \\ 0 & 0 & 0 \\ 0 & 0 & \gamma \end{bmatrix} + \frac{1}{\omega}\begin{bmatrix} 0 & 0 & \alpha \\ 0 & 0 & \alpha^* \\ \alpha^* & \alpha & 0 \end{bmatrix} + \frac{1}{\omega^2}\begin{bmatrix} \beta & -\beta & 0 \\ -\beta & \beta & 0 \\ 0 & 0 & 0 \end{bmatrix} + ...$$

where $\alpha = i\gamma\Omega$ and $\beta = 3\gamma\Omega^2/2$.

Similar to the analysis of two-level system, we will compute the eigenvalues perturbatively, and at any given order n, we will cut off the terms of the order $\mathcal{O}(\omega^{-(n+1)})$, and modify the non-positive terms. At the first order the eigenvalues read

$$\begin{aligned} \lambda_1^{(1)} &= \gamma(1 + \mathcal{O}(\omega^{-2})), \\ \lambda_2^{(1)} &= \gamma(\mathcal{O}(\omega^{-2})), \\ \lambda_3^{(1)} &= 0. \end{aligned} \tag{5.30}$$

The corrected eigenvalues thus read $\tilde{\lambda}^{(0)} = \{\gamma, 0, 0\}$, which along with the obtained eigenvectors construct the coefficient matrix $\tilde{\mathcal{C}}_1$ as

$$\tilde{\mathcal{C}}_1 = \gamma \begin{bmatrix} \Omega^2/\omega^2 & -\Omega^2/\omega^2 & i\Omega/\omega \\ -\Omega^2/\omega^2 & \Omega^2/\omega^2 & -i\Omega/\omega \\ -i\Omega/\omega & i\Omega/\omega & 1 \end{bmatrix}.$$

By describing the dynamics in the frame in which the effective Hamiltonian $\mathcal{H}_1$ is diagonal, we can rewrite the effective generator $\mathfrak{L}_1$ as

$$\tilde{\mathfrak{L}}_1(T)/T[\circ] = -i[\omega_0\tilde{n}, \circ] + \gamma\mathcal{D}_{\tilde{n}}[\circ], \tag{5.31}$$

defined in terms of

$$\tilde{n} \;=\; U_\Omega \hat{n} U_\Omega^\dagger$$

with $U_\Omega = \exp[i\frac{\Omega}{\omega}(a+a^\dagger)]$. Similar to the case of driven two-level system, here the difference between the driven and the un-driven system is a perturbative transformation of the operators $\{a, a^\dagger, \hat{n}\} \to \{\tilde{a}, \tilde{a}^\dagger, \tilde{n}\}$, *i.e.* $\tilde{a} = a - i\Omega/\omega\mathbb{I}$.

The eigenvalues of $\mathcal{C}_2$ in second order read $\lambda_1^{(2)} = \{\gamma(1+\frac{\Omega^2}{\omega^2}), \frac{2\gamma\Omega^2}{\omega^2}, 0\}$, and since they are all positive, no modification is required. Based on the eigenvectors corresponding to $\lambda_1^{(2)}$ and $\lambda_2^{(2)}$, the effective dissipative processes read

$$\begin{aligned} \mathcal{P}_1^{(2)} &= \tilde{n} - \frac{\Omega^2}{\omega^2}\hat{n} \\ \mathcal{P}_2^{(2)} &= \frac{i}{\sqrt{2}}(\tilde{a}^\dagger - \tilde{a}) \equiv \tilde{p}. \end{aligned} \tag{5.32}$$

By modifying the eigenvalue $\lambda_1^{(2)}$ as described in Subsec. A.2.2, one can rewrite the effective generator purely in the transformed space as

$$\mathfrak{L}_2(T)/T[\circ] = \gamma\left(1-\frac{\Omega^2}{2\omega^2}\right)^2 \mathcal{D}_{\tilde{n}}[\circ] + 4\gamma\frac{\Omega^2}{\omega^2}\mathcal{D}_{\tilde{p}}[\circ]\,.$$

One can see that in second order, the dissipation rate in comparison with first order approximation is reduced by a factor of $(1-\frac{\Omega^2}{2\omega^2})^2$. There is a second process $\tilde{\gamma}_2\mathcal{D}_{\tilde{p}}$, which describes the diffusion in real space [47, 48] with rate $\tilde{\gamma}_2 = 4\gamma\frac{\Omega^2}{\omega^2}$.

The insets (a) and (b) of Fig 5.3 depict the performance of the obtained approximations for the specific parameters $\Omega/\omega = \gamma/\Omega = 1/8$. Inset (a) shows the ground state ($a|0\rangle = 0$) population for the initial condition $\varrho(0) = |0\rangle\langle 0|$. Similarly to inset (a) of Fig.(5.1), $\mathfrak{L}_1$ induces dynamics that is evidently not completely positive, and therefore, it violates the algebraic structure associated with the dynamics of open quantum systems. The complete

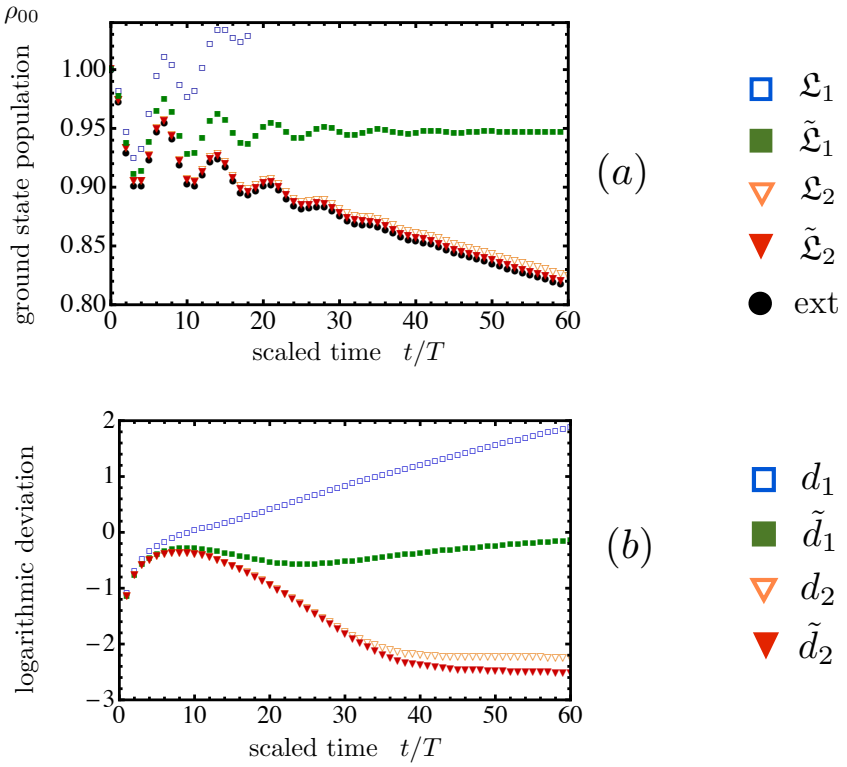

Figure 5.3: Figure (a) depicts the ground state population of a driven, dissipative harmonic oscillator as function of time (in multiples of T) for the specific parameters $\Omega/\omega = \gamma/\Omega = 1/8$. Empty squares (blue) and triangles (orange) depict the approximation in first and second order, and full squares (green) and triangles (red) depict the corresponding completely positive approximations; the exact solution is depicted in full circles (black). Figure (b) depicts the comparison defined in Eq. (5.28) of the propagators in approximation and their extensions that demonstrates the added value of the present completely positive, approximate maps.

positivity of the dynamics is retrieved by employing the corrected generator $\tilde{\mathfrak{L}}_1$, which yields an improvement in the accuracy of the approximation during the first few driving periods. Similarly to the two-level system, the rendered improvement does not last long as the accuracy of the approxi-

mation drops after few driving periods. The second order corrected generaor $\tilde{\mathfrak{L}}_2$ overcomes this flaw by inducing a much more accurate approximation of the exact dynamics than $\mathfrak{L}_2$. Similarly to inset of Fig.(5.1), inset (b) demonstrates that substantial improvement in accuracy is obtained through the use of corrected generators[1].

5.5 Lambda System

In this section we will provide a brief description of driven three-level systems or *Lambda systems*, and will briefly discuss the improvement in approximating the dynamics yielded by the proposed correction scheme.

The Lambda system is a three-level system including two ground states $|1\rangle, |2\rangle$ and an excited state $|3\rangle$. Here we consider the example in which one is interested in simulating a dynamics which encodes the transition $|1\rangle \leftrightarrow |2\rangle$; that is the Raman transition within the ground state manifold via driving the transitions $|1\rangle \leftrightarrow |3\rangle$ and $|2\rangle \leftrightarrow |3\rangle$. The Hamiltonian encoding such a transition in the interaction picture reads

$$H_{ls}(t) = \Omega e^{i\Delta t}(|3\rangle\langle 1| + |3\rangle\langle 2|) + \text{H.c.} \tag{5.33}$$

where Ω is the Rabi frequency, and Δ is the detuning from the excited state $\Delta = \omega - \omega_0$, with ω being the fundamental driving frequency, and ω_0 being the resonance frequency of the bare system. In the presence of dephasing process with rate γ , the time-dependent generator $\mathcal{L}_{ls}(t)$ reads

$$\mathcal{L}_{ls}(t)[\circ] \;\; = \;\; -i[\mathcal{H}_{ls}(t), \circ] + \gamma \mathcal{D}_{\mathscr{G}_8}[\circ] \tag{5.34}$$

where $\{\mathscr{G}_j\}$ is the set of Gell-Mann matrices [49] *see* Sec. B.1, and $\mathscr{G}_8$ representing the phenomenological description of the dephasing process within

[1]For harmonic oscillator Eq. (5.28) is evaluated in the subspace spanned by the lowest four oscillator eigenstates with negligible induced error.

the Lambda system. *see* Fig.(5.4).

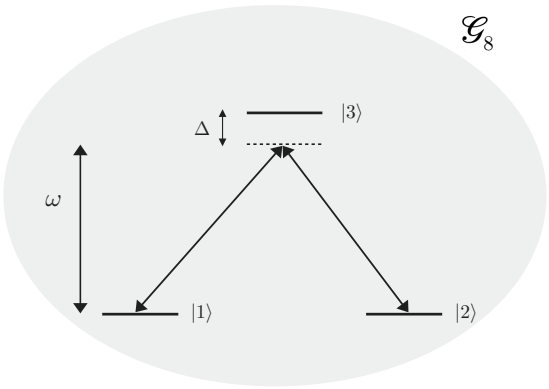

Figure 5.4: Level scheme of a dissipative driven degenerate lambda system; simulating the Raman transition in the ground state manifold, $|1\rangle \leftrightarrow |2\rangle$ via driving the transition $|1\rangle \leftrightarrow |3\rangle$ and $|2\rangle \leftrightarrow |3\rangle$.

The resulting effective Hamiltonian in the first order approximation reads

$$\mathcal{H}_n = \frac{\Omega^2}{\Delta}\big(\sqrt{3/2}\mathscr{G}_8 + 3/\sqrt{2}\mathscr{G}_3 + \sqrt{2}\mathscr{G}_6\big) + \mathcal{O}(\Delta^{-2}) \tag{5.35}$$

and the effective coefficient matrix encoding the dissipation reads

$$\mathcal{C}_n \;=\; \gamma \begin{bmatrix} 1 & \frac{\sqrt{3}\Omega}{\Delta} \\ \frac{\sqrt{3}\Omega}{\Delta} & 0 \end{bmatrix} + \mathcal{O}(\Delta^{-2})$$

in the subspace $\{\mathscr{G}_8, \mathscr{G}_4\}$ [2]. By preserving the eigenvalues up to the or-

[2]The size of the matrix grows as one includes higher order terms; it is however, a bounded 9×9 matrix in the space of Gell-Mann matrices.

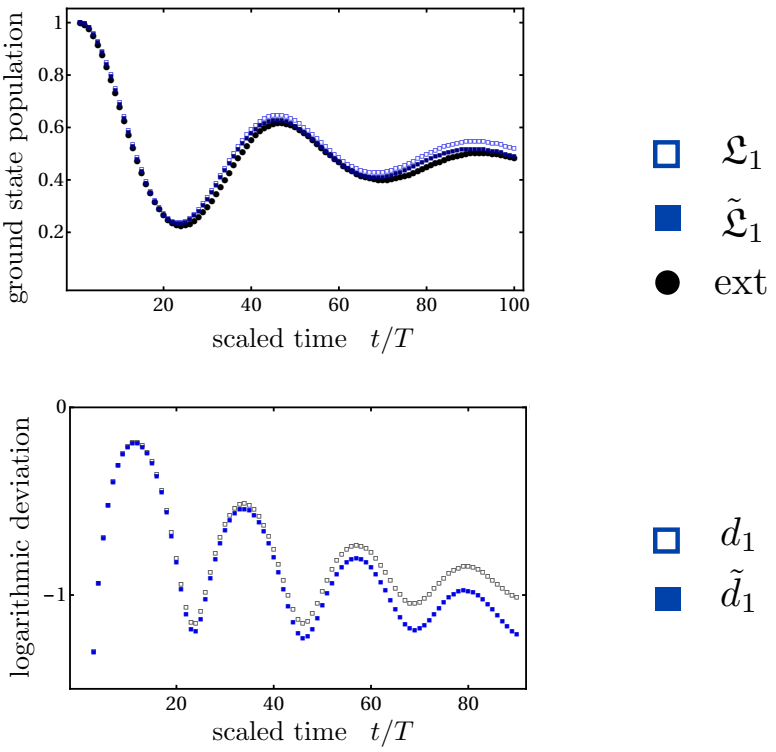

Figure 5.5: Figure (a) depicts the ground state population of a driven, dissipative lambda system as function of time (in multiples of T) for the specific parameters $\Omega/\Delta = \gamma/\Omega = 1/10$. The empty squares depict the induced dynamics at the first order, filled squares depict the corresponding completely positive dynamics, and the filled circles depict the exact dynamics. Figure (b) depicts the comparison defined in Eq. (5.28) of the propagators.

der $\mathcal{O}(\Delta^{-1})$, and cutting off the higher order terms, this matrix is positive-semidefinite with eigenvalues $\{\tilde{\lambda}_1^{(1)} = \gamma, \tilde{\lambda}_2^{(1)} = 0\}$. Based on the corresponding eigenvectors, the effective generator reads

$$\begin{aligned} \tilde{\mathfrak{L}}_1[\circ] &= -i[\mathcal{H}_1, \circ] + \gamma \mathcal{D}_{\mathcal{P}_1}[\circ] \quad \text{with} \\ \mathcal{P}_1 &= \mathscr{G}_8 + \frac{\sqrt{3}\Omega}{\Delta}\mathscr{G}_4. \end{aligned} \tag{5.36}$$

Fig.(5.5) depicts a comparison of the dynamics induced by the effective generators $\mathfrak{L}_1$, in first order, its corrected counterpart $\tilde{\mathfrak{L}}_1$ and the exact effective dynamics for the specific parameters $\Omega/\Delta = \gamma/\Omega = 1/10$. Inset (a) shows the population of ground state $|1\rangle$ with $\varrho(0) = |0\rangle\langle 0|$ as initial condition. As one can see the corrected generator induces a slight improvement in approximating the dynamics. This also can be seen in the inset (b) which depicts the deviation of the approximate dynamics from the exact dynamics.

In this chapter we constructed valid approximate solutions which describe the dynamics of driven open quantum systems based on the series expansion methodology. The fundamental property of the dynamics namely, the condition of complete positivity is installed in the approximation using the proposed correction scheme. We studied the approximate dynamics of several dissipative driven systems including two-level system, Lambda-system and harmonic oscillator based on the proposed scheme, and we found significant improvement in the accuracy of the approximations. Next, we will be investigating the dynamics of another driven dissipative system namely the MS gate in the context of open system dynamics. By obtaining the approximate dynamics we will try to optimally shape this approximate behaviour towards an ideal dynamics, that is the gate dynamics in the absence of dissipation.

Chapter 6

Pulse Shaping

In the previous chapter, we investigated the behaviour of the driven open quantum systems by constructing approximate models based on series expansion methods. In this chapter, we extend this conceptual model to analyse and control the behaviour of dissipative trapped ions, in particular, the dynamics of entangling gates in the presence of motional decoherence.

6.1 Irreversible Processes

As we discussed in chapter 4, the MS gate is induced by two driving fields that are slightly detuned with respect to the red and blue sideband transitions respectively. The corresponding Hamiltonian reads

$$\mathcal{H}(t) = (\Upsilon(t)\, a + \Upsilon^*(t)\, a^\dagger)\, \mathcal{S}_x \,,$$

in terms of the creation and annihilation operators a and $a^\dagger$ of phonons in the bus mode and the collective operator $\mathcal{S}_x = \sum_j \sigma_x^{(j)}$ where $\sigma_x^{(j)}$ induces transitions between the two qubit states of the j-th ion. Here the time-dependent function $\Upsilon(t)$ is a generic representation of the mathematical relation between the driving field amplitudes and the symmetric detunings from the sideband transitions. As we discussed in Chapter 4, in the

minimal form it equals $\eta\Omega\exp(i\delta t)$ with the Lamb-Dicke parameter η, the Rabi frequency Ω and the detuning δ [3], but, in the following, we will consider more general time dependencies.

By applying Magnus series the propagator induced by $\mathcal{H}(t)$ can be written as

$$\mathcal{U}(t) = \exp\left(-i\big((f(t)a + f^*(t)a^\dagger)\mathcal{S}_x - g(t)\mathcal{S}_x^2\big)\right) \tag{6.1}$$

with

$$\begin{aligned} f(t) &= \int_0^t dt' \Upsilon(t') \\ g(t) &= \Im \int_0^t dt' \Upsilon(t') f^*(t'). \end{aligned} \tag{6.2}$$

At instances at which f vanishes, this describes the dynamics induced by the spin-spin-type interaction $\mathcal{S}_x^2$ independently of the the motional state of the bus mode. Due to this feature the ground-state cooling of the ions is no longer required, and high fidelity multi-qubit quantum gates even with incoherent, thermal states have been experimentally implemented [50–52]. For the realization of fault tolerant quantum computation, a discipline of performing quantum gates on qubits encoded in quantum error-correcting codes however, incoherent processes during the gate operation are a limiting factor [53]. In the course of the gate operation the qubits and motional degrees of freedom get correlated as mathematically encoded within the term $(f(t)a + f^*(t)a^\dagger)\mathcal{S}_x$ in Eq.(6.1) so that dissipation of the ions' motion affects the coherence of the qubits. Predominant dissipative processes effecting the ion's motional degree of freedom are thermalization and dephasing that can be modelled with a Master equation characterized by a generator [25]

$$\mathcal{L}[\circ] = -i[\mathcal{H}(t), \circ] + \sum_{j=+,-,d} \gamma_j \mathcal{D}_{E_j}[\circ]\,. \tag{6.3}$$

The first term $-i[\mathcal{H}(t), \circ]$ describes coherent dynamics and the dissipator $\sum_{j=+,-,d} \gamma_j \mathcal{D}_{E_j}[\circ]$ encodes the irreversible processes which can be phe-

nomenologically represented in terms of the operators $E_- = a$ and $E_+ = a^\dagger$ for thermalization and $E_d = a^\dagger a = \hat{n}$ for dephasing.

It is convenient to describe the dynamics in the frame induced by the coherent part of the generator $\mathcal{U}(t)$ given in Eq.(6.2). Since this is the exact solution to the dynamics of the coherent version of the gate, by transforming to this induced frame, the remaining terms simply encode the irreversible processes, and the optimisation problem is reduced to the minimisation of all these remaining terms except the identity operator $\mathbb{I}$, which encodes the entangling operation. The transformed time-dependent generator $\tilde{\mathcal{L}}(t)$ which encodes a pure irreversible dynamics, reads

$$\tilde{\mathcal{L}}(t)[\circ] = \sum_j \gamma_j \mathcal{D}_{\tilde{E}_j(t)}[\circ] \tag{6.4}$$

with

$$\begin{aligned} \tilde{E}_- &= a - if^*(t)\mathcal{S}_x \,, \\ \tilde{E}_+ &= a^\dagger + if(t)\mathcal{S}_x \,, \\ \tilde{E}_d &= \hat{n} + i(af(t) - a^\dagger f^*(t))\mathcal{S}_x + |f(t)|^2\mathcal{S}_x^2 \,. \end{aligned} \tag{6.5}$$

Since during the gate operation internal and external degrees of freedom of the ions get correlated, the dissipative operators $\tilde{E}_j$ directly affect both qubits and motional degrees of freedom, which is the formal manifestation of the fact that motional decoherence affects the qubits during gate operation.
The propagator induced by the time-dependent generator $\tilde{\mathcal{L}}(t)$ can thus be approximated using series expansion based on the Magnus series

$$\tilde{\mathcal{E}}(t) \simeq \exp\left(\int_0^t dt' \tilde{\mathcal{L}}(t') + \frac{1}{2}\int_0^t dt' \int_0^{t'} dt'' [\tilde{\mathcal{L}}(t'), \tilde{\mathcal{L}}(t'')] + \mathcal{O}(\gamma^3) \right). \tag{6.6}$$

As we mentioned earlier, the term in the exponent represents the decoherence processes in the system, absence of which would result in identity *i.e.*

$\tilde{\mathcal{E}}(t) = \mathbb{I}$, characterising the ideal entangling operation. In state of the art experiments however, the transition rates are sufficiently small such that $\gamma_j T \ll 1$, where T is the gate duration. The infidelity $\mathcal{I}$ of the gate operation thus can be characterized in leading order by the magnitude of the map

$$\Xi(\circ) = \mathrm{Tr}_{\mathcal{B}} \int_0^T dt' \; \tilde{\mathcal{L}}(t')[\circ \otimes \varrho_{\mathcal{B}}] \; , \tag{6.7}$$

where $\mathrm{Tr}_{\mathcal{B}}$ denotes the trace over the bus mode with the density operator $\varrho_{\mathcal{B}}$. In practice, we define the measure for infidelity as $\mathcal{I} = \| \; \zeta \; \|_2$ in terms of the 2-norm of the coefficient matrix ζ [54], with elements related to the reduced map Ξ which can be represented as

$$\Xi(\circ) = \sum_{ij} \; \zeta_{ij} \; \xi_i \; \circ \; \xi_j^{\dagger} \tag{6.8}$$

where the set of operator $\{\xi_j\}$ form a orthonormal basis, and are defined as $\xi_0 = \mathbf{1}$ and

$$\xi_i = \binom{N}{i}^{-\frac{1}{2}} \sum_{1 \leq j_1 < \ldots < j_i \leq N} \sigma_x^{(j_1)} \ldots \sigma_x^{(j_i)}$$

for $i = 1, 2, 3, 4$.

Let us consider the case where the only dissipative process is the process of heating which as we will discuss later is the main source of noise in surface-electrode ion traps. By tracing over the motional degrees of freedom the error channel Ξ can be constructed in terms of the following dissipative processes

$$\Xi[\circ] \quad : \quad (\mathfrak{F}\{f; a\} + \mathfrak{F}\{f^*; a^{\dagger}\})(-i[\xi_1, \circ]) + \mathfrak{F}\{f f^*; \mathbb{I}\}\mathcal{D}_{\xi_1}[\circ],$$

where the functional $\mathfrak{F}$ is a bi-linear map defined as

$$\mathfrak{F}\{\odot; \bullet\} = (\int_0^T \odot \, dt)(\mathrm{Tr}[\, \bullet \, \varrho_{\mathcal{B}}]). \tag{6.9}$$

As one can see the error channel can be read off as an infinitesimal reversible channel weighted by the magnitude of the functional $\mathfrak{F}\{f;a\} + \mathfrak{F}\{f^*;a^\dagger\}$, and an infinitesimal irreversible channel weighted by the magnitude of the functional $\mathfrak{F}\{ff^*;\mathbb{I}\}$. So one can construct the ζ-matrix in terms of these functionals, and the basis operators $\{\xi_0,\xi_1,\xi_2\}$ as following

$$\zeta \;=\; h(\gamma_+)\circ\begin{bmatrix} \mathfrak{F}\{ff^*;\mathbb{I}\} & \mathfrak{F}\{f;a\}+\mathfrak{F}\{f^*;a^\dagger\} & \mathfrak{F}\{ff^*;\mathbb{I}\} \\ \mathfrak{F}\{f;a\}+\mathfrak{F}\{f^*;a^\dagger\} & \mathfrak{F}\{ff^*;\mathbb{I}\} & 0 \\ \mathfrak{F}\{ff^*;\mathbb{I}\} & 0 & 0 \end{bmatrix},$$

where h is a constant matrix encoding the heating rate γ_+ as

$$h(\gamma_+) \;=\; \gamma_+\begin{bmatrix} -N & -i & -1 \\ i & N & 0 \\ -1 & 0 & 0 \end{bmatrix},$$

and $\circ$ denotes the entry-wise product, which is referred to as the *Hadamard product*. The norm of ζ-matrix will be the measure of infidelity in our analysis of dissipative quantum gates. According to the Eq.(6.9), the gate infidelity depends on the state of the bus mode within the construction of the functionals $\{\mathfrak{F}\}$ as

$$\mathfrak{F}\{\odot;\hat{\mathcal{O}}(a,a^\dagger)\} = (\int_0^T \odot\, dt)\langle\hat{\mathcal{O}}(a,a^\dagger)\rangle, \tag{6.10}$$

where $\hat{\mathcal{O}}$ is an operator-valued function of a and $a^\dagger$. In our analysis however, we have approximated the error channel to the first order in γ, and this results in the presence of only lower powers of the operators $a, a^\dagger$ in the approximate dynamics *i.e.* $\langle a\rangle$, $\langle a^\dagger\rangle$, $\langle\hat{n}\rangle$, $\langle a^2\rangle$, and $\langle {a^\dagger}^2\rangle$. In order to minimize the error channel one might optimize the magnitude of the functionals $\{\mathfrak{F}\}$ in which case the control scheme would be dependent on the state of the bus mode and overall on the environment model. Since, in

practice, a control scheme which is independent of the exact form of the dissipation is desirable, we will refrain from optimizing the gate infidelity for very specific situations, but rather target solutions that yield good performance largely independent of bus mode properties. In the following section, we will search for pulse patterns $\Upsilon(t)$ for which the minimal magnitudes of the functionals $\{\mathfrak{F}\}$, and eventually, suppressed values of gate infidelity encoded in the matrix ζ can be obtained.

6.2 Series Analysis

As deviations from perfect gate operations result from qubit-phonon entanglement as characterized by ζ-matrix in Eq.(6.1), one would expect to achieve high fidelities by minimizing the deviations of $||\zeta||_2$ from 0. Let us represent the pulse $\Upsilon(t)$ in terms of the following series expansion

$$\Upsilon_p = \sum_{j=1}^{m} c_j \omega \exp(ij\omega t)$$

where ω is the fundamental detuning frequency of the radiation field, and the set $\{c_j\}$ is the set of unitless, complex amplitudes. With such an explicit parameterisation we can apply optimal control techniques in order to maintain the performance of the gate while suppressing dissipative effects; that is, the optimization problem to be solved can be set up as

$$\min_{\{c_j\}} \left(\parallel \zeta \parallel_2 \;\middle|\; \mathcal{U}(T) = \exp(-i\Phi(T)\mathcal{S}_x^2) \right).$$

where $\Phi(T)$ is the phase of the entangling operation which should be set to $\pi/8$ in order to obtain a maximally entangled GHZ state. As we discussed in the previous section the infidelity can be deconstructed in terms of a set of functionals $\{\mathfrak{F}\}$ which can be expanded in terms of polynomials based

on the driving amplitudes *e.g.*

$$\begin{aligned} \mathfrak{F}\{f;\bullet\} &\propto \sum_{j=1}^{m} c_j/j \\ \mathfrak{F}\{ff^*;\bullet\} &\propto \sum_{j}^{m} c_j c_j^*/j^2 + \sum_{j,k=1}^{m} c_j c_k^*/jk \\ &\vdots \end{aligned} \tag{6.11}$$

For certain class of such polynomials, there exist combinations of $\{c_j\}$ which satisfy $\mathfrak{F} = 0$, whereas other class of polynomials are always non-negative for non-vanishing pulse $\Upsilon(t)$. Therefore, the optimisation problem can be expressed in terms of two sets of zero and non-zero functionals $\{\mathfrak{F}\}_{=0}$ and $\{\mathfrak{F}\}_{\neq 0}$ respectively as

$$\min_{\{c_j\}} \left(\left\{ \mathfrak{F} \right\}_{\neq 0} \middle| \left\{ \mathfrak{F} \right\}_{=0} = 0 \ ; \ \mathcal{U}_{\mathcal{K}}(T) = e^{-i\Phi(T)\mathcal{S}_x^2} \right).$$

where Φ is the desired phase of the entangling operation. In the following we will consider two environment models in which decoherence occurs. In the first model we will consider the case where the predominant process is thermalisation, and in the second model we will include the dephasing processes in addition to the thermalisation.

6.2.1 Thermalisation

Let us consider the case where the dominant dissipative processes are phenomenologically described in terms of the operators $\tilde{E}_+$ for heating and $\tilde{E}_-$ for decay. The ζ-matrix then reads

$$\zeta \;=\; h(\gamma_-,\gamma_+)\circ\begin{bmatrix} \mathfrak{F}\{ff^*;\mathbb{I}\} & \mathfrak{F}\{f;a\}+\mathfrak{F}\{f^*;a^\dagger\} & \mathfrak{F}\{ff^*;\mathbb{I}\} \\ \mathfrak{F}\{f;a\}+\mathfrak{F}\{f^*;a^\dagger\} & \mathfrak{F}\{ff^*;\mathbb{I}\} & 0 \\ \mathfrak{F}\{ff^*;\mathbb{I}\} & 0 & 0 \end{bmatrix},$$

where h is defined as

$$h(\gamma_-,\gamma_+) \;=\; \begin{bmatrix} -N(\gamma_-+\gamma_+) & i(\gamma_--\gamma_+) & -(\gamma_-+\gamma_+) \\ i(\gamma_+-\gamma_-) & N(\gamma_-+\gamma_+) & 0 \\ -(\gamma_-+\gamma_+) & 0 & 0 \end{bmatrix}.$$

Here one can see that the functional to be minimized is $\mathfrak{F}\{ff^*;\mathbb{I}\}$, with corresponding constraint $\mathfrak{F}\{f;\bullet\}=0$. By applying the method of Lagrange multipliers, the optimization problem is mapped to the problem of solving a set of nonlinear equations

$$\min_{\{c_j\}}\left(\sum_{j=1,k}^{m}\frac{c_jc_k^*}{jk}+\sum_{j}^{m}\frac{c_jc_j^*}{j^2}\;\middle|\;\sum_{j=1}^{m}\frac{c_j}{j}=0\,,\sum_{j=1}^{m}\frac{c_jc_j^*}{j}=\frac{1}{16}\right).$$

Since the first term in the functional to-be-optimised is equal to the square of the constraint *i.e.* $\sum_{j=1,k}^{m}\frac{c_jc_k^*}{jk}=|\sum_{j=1}^{m}\frac{c_j}{j}|^2$, the final optimisation problem can be reduced to

$$\min_{\{c_j\}}\left(\sum_{j}^{m}\frac{c_jc_j^*}{j^2}\;\middle|\;\sum_{j=1}^{m}\frac{c_j}{j}=0\,,\sum_{j=1}^{m}\frac{c_jc_j^*}{j}=\frac{1}{16}\right).$$

from which the optimal solution c_j^{opt} [55], reads

$$c_j^{opt}=\frac{j\lambda_0}{1-j\lambda_1}\;\text{ with }\;\lambda_0\lambda_0^*=\frac{1}{16}\left(\sum_{j=1}^{m}\frac{j}{(1-j\lambda_1)^2}\right)^{-1}. \tag{6.12}$$

Clearly $\lambda_0\in\mathbb{C}$, but without loss of generality, here we will restrict it to be a real number, and therefore the optimal amplitudes c_j^{opt} can be chosen real.

m	2	3	4	5	6
λ_1	$\frac{2}{3}$	$\frac{(6-\sqrt{3})}{11} \simeq 0.388$	$\frac{(5-\sqrt{5})}{10} \simeq 0.276$	0.215	0.177
c_1^{opt}	-0.144	-0.032	-0.015	-0.009	-0.006
c_2^{opt}	0.288	-0.179	-0.051	-0.026	-0.016
c_3^{opt}	0	0.368	-0.201	-0.064	-0.034
c_4^{opt}	0	0	0.435	-0.218	-0.073
c_5^{opt}	0	0	0	0.493	-0.231
c_6^{opt}	0	0	0	0	0.546

Table 6.1: Numerical values of optimal amplitudes c_j^{opt} and λ_1 defined in Eq.(6.12) and Eq.(6.13) respectively for up to $m = 6$ frequencies. Exact values of λ_1 for $m = 5$ is $\lambda_1 = \frac{1}{548}(3(75+\sqrt{145}) - \sqrt{10830+802\sqrt{145}})$ and for $m = 6$ is $\lambda_1 = \frac{1}{252}(98 + 7\sqrt{7} - \sqrt{2891+868\sqrt{7}})$.

This can be understood form Eq.(6.12) which indicates that the pulse pattern or in other worlds, the relative phases of the driving amplitudes which are essential in satisfying the constraint and minimising the infidelity, is totally independent of λ_0, which only effects the global phase of the pulse, and that is not a relevant quantity in the optimisation procedure. The other Lagrange coefficient λ_1 which satisfies the equation

$$\sum_j^m (1 - j\lambda_1)^{-1} = 0 \,. \tag{6.13}$$

is real. But as one can see, this equation is a polynomial with $m-1$ roots, where j^{th} root is positioned in the interval $(1/j, 1/(j+1))$ with $j = 1, ..., m-1$. We need to choose the root which minimises the term $\sum_j^m \frac{c_j c_j^*}{j^2}$. This term however, is a monotonically increasing function in the interval $[1/m, 1]$, and therefore, its minimal value corresponds to the minimal root of the Eq.(6.13). For $m \leq 6$, this root can be obtained analytically, and for spectrally broader pulses, *i.e.* larger values of m this root can be found numerically; the solutions $\{\lambda_1, c_j^{opt}\}$ for $m \leq 6$ are depicted in Table 6.1.

Fig.(6.1) depicts the highest frequency components of the optimised

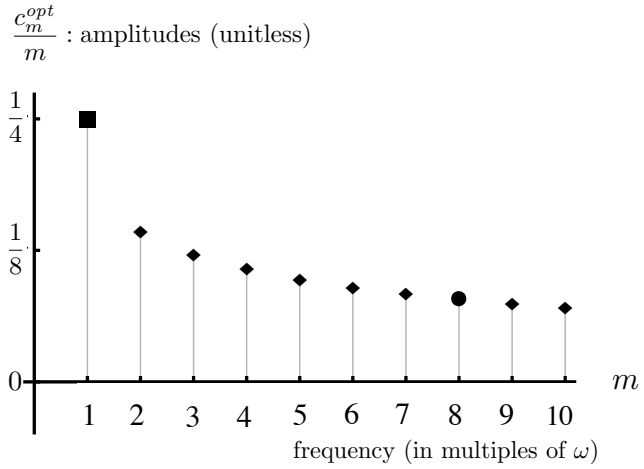

Figure 6.1: The filled square depicts the amplitude for a monochromatic pulse and the diamonds depict the amplitude of the highest (and dominant) frequency component for c_m^{opt}/m for m ranging from 2 to 10.

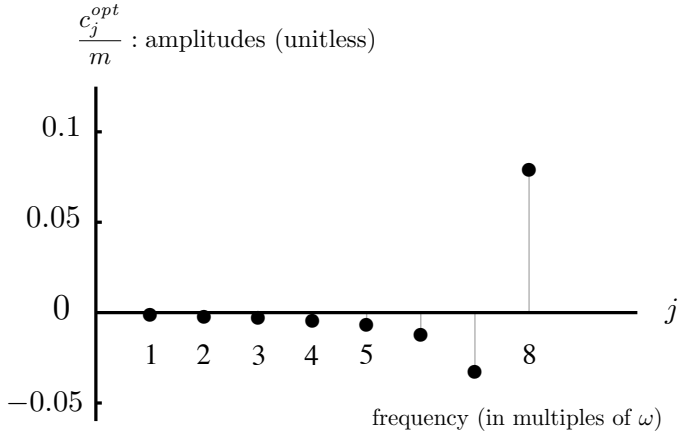

Figure 6.2: Here, we depict the amplitudes c_j^{opt}/m of the optimal pulse (Eq.(6.12)) with $m = 8$ frequency components. The amplitude of the highest frequency component is always dominant and phase shifted as compared to all other amplitudes. The conservative comparison $m\omega$ =const. implies that gate duration increases with m and the amplitudes c_j^{opt}/m get lower with increasing m as depicted here.

pulse amplitudes as a function of the number of frequencies m. As the number of driving frequencies m increases, the magnitude of the amplitudes decreases. Fig.(6.2) depicts the optimised pulse pattern for a fixed number of driving frequencies *e.g.* $m = 8$. The amplitudes increase as the index j corresponding to the frequency component $j\omega$ grows. As the inset shows, there is a phase difference of π between the amplitudes corresponding to the highest frequency component, which generates the leading contribution to the gate performance, and all the remaining amplitudes. Due to this phase-difference, the interference among all these amplitudes becomes destructive, which is formally imposed by the constraint $\mathfrak{F}\{f;\bullet\} = 0$, and this leads to the suppression of qubit-phonon coupling encoded within the function $f(t)$ in Eq.(6.1).

In order to carry out an unbiased comparison between the performances of conventional and optimised polychromatically driven gates, one should respect the two following rules. First, the infidelity induced by the decoherence of the motional degree of freedom, can always be reduced by increasing the fundamental detuning frequency ω, which itself necessitates the incorporation of stronger driving amplitudes. This would lead to increased off-resonant excitations of additional transitions, and eventually will have detrimental impact on the gate fidelity. In the following comparison we will thus always consider the case that the detuning δ of the monochromatic pulse equals the highest frequency $m\omega$ of the polychromatic pulse, so that the polychromatic pulse contains no higher frequencies than the monochromatic pulse, and the period of the polychromatic pulse is a factor of m longer than that of the monochromatic pulse. Second, the infidelity induced by motional dissipation can also be suppressed arbitrarily by prolonging the gate duration [53]; that is, for a fixed detuning, prolonging the gate duration or increasing the number of excursions along the loop in the phase space would result in the reduced gate infidelity induced by the motional dissipation. Thus, we will compare the infidelity of the conventionally driven gate with a duration of m driving periods with

the optimised polychromatically driven gate with a duration of one driving period *i.e.* $T = 2\pi/\omega$.

By imposing the previous rules on the conduct of the comparison, we have not explicitly put any restriction on the magnitudes of the required amplitudes. Since, there might be limitations on the achievable range of the the driving amplitudes from an experimental point of view, it is thus important to assess the difference between the required amplitudes for the implementation of the conventional and polychromatic gates. The intensity of the conventional monochromatic pulse reads $\mathcal{E}_{con} = m\omega^2/16$ as compared to the intensity $\mathcal{E}_{pol} = \sum_{j=1}^{m}(c_j^{opt}\omega)^2$ with c_j^{opt} given in Eq.(6.12) for the optimised polychromatic case. These intensities are of comparable magnitude, but one can see that $\mathcal{E}_{pol}$ never exceeds $\mathcal{E}_{mon}$; the exact value of $\mathcal{E}_{pol}$ is determined by the smallest root of Eq.(6.13), which lies in the interval $[1/m, 1/(m-1)]$. In this interval, the sum $\sum_{j=1}^{m}(c_j^{opt}\omega)^2$ is a monotonically decreasing function of λ_1. Therefore, one can obtain an upper bound to the intensity by replacing the value of λ_1 by $1/m$, which by using Eq.(6.12) results in

$$\mathcal{E}_{pol} \leq \lim_{\lambda\to\frac{1}{m}} \frac{\omega^2 \sum_{j=1}^{m} \frac{j^2}{(1-j\lambda)^2}}{16 \sum_{j=1}^{m} \frac{j}{(1-j\lambda)^2}} = \lim_{\lambda\to\frac{1}{m}} \frac{\omega^2 \frac{m^2}{(1-m\lambda)^2}}{16 \frac{m}{(1-m\lambda)^2}} = \frac{m\omega^2}{16} = \mathcal{E}_{con}\ . \qquad (6.14)$$

That is, in the following comparison, the polychromatic pulse will always be weaker in intensity, and contains no higher frequency components than the conventional monochromatic pulse.

Fig.(6.3) depicts the improvement R defined in terms of the ratio of the gate infidelities $\mathcal{I}$ for an optimized pulse and a monochromatic pulse, $\mathcal{I}_m/\mathcal{I}_p$. Circles correspond to the environment model for which ($\gamma_+ = \gamma_- > 0$, $\gamma_d = 0$, with rates γ_+, γ_- and γ_d defined in Eq.(6.3)), and the improvement is plotted as a function of the number of frequencies m in the pulse Υ_p. The bus mode is assumed to be in its ground state. The minimum number of frequencies by which the constraint $\mathfrak{F}\{f;\bullet\} \propto \sum_j c_j/j = 0$ can be satisfied is two, and as the Fig.(6.3) shows, a pulse with only two frequen-

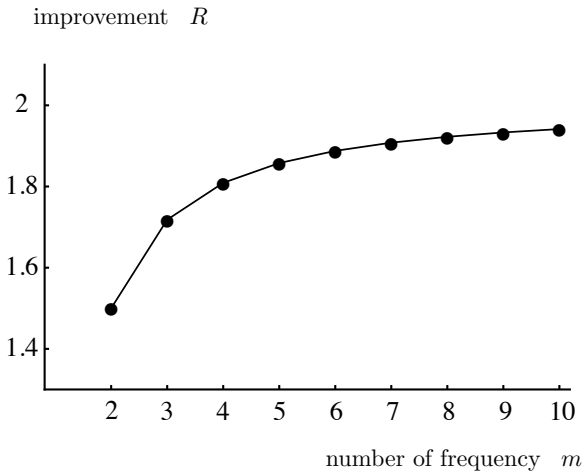

Figure 6.3: Improvement $R = \mathcal{I}_m/\mathcal{I}_p$ of gate infidelities ($\mathcal{I}_m$ and $\mathcal{I}_p$ for monochromatic and polychromatic driving) in terms of number of the frequencies in an optimized polychromatic pulse. Circles correspond to finite thermalization with equal rates and vanishing dephasing, $\gamma_+ = \gamma_- > 0, \gamma_d = 0$.

cies induces an improvement of a factor of 1.5. By satisfying the constraint $\mathfrak{F}\{f;\bullet\} = 0$, the yielded improvement becomes absolutely insensitive to the phonon mode excitation $\langle a \rangle$ as can be understood in terms of the coefficient matrix ζ given in Eq.(6.12). A remarkable aspect of this optimisation is that this improvement in the gate performance is also independent of the thermalisation rates as well as the number of the ions N, and therefore by increasing the number of qubits in the ion trap, the induced improvement in the gate performance will be maintained. [1]

By including more frequency components we observe that the improvement of the suppression in the gate infidelity, increases as a hyperbolic function. In order to understand the asymptotic behaviour of the improvement it would be sensible to represent the optimised gate dynamics in the phase-space. As we discussed in chapter 4, the entangling gate operation

[1]We note that here we have taken into account only one motional mode

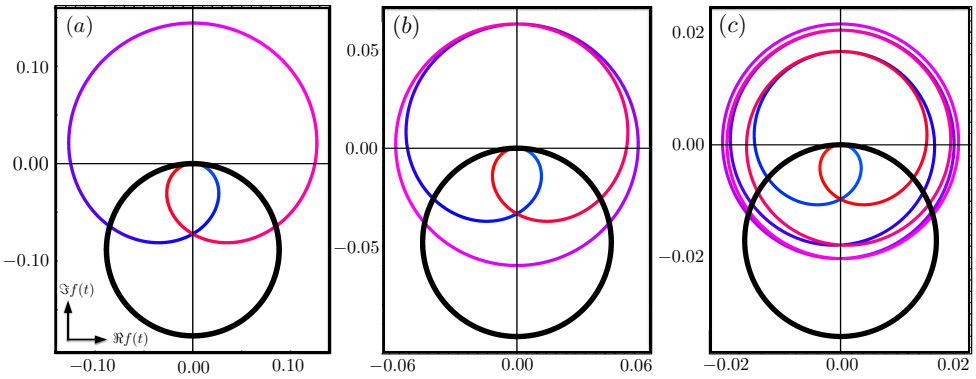

Figure 6.4: Phase-space trajectories of the bus mode characterized by $\Re f(t)$ and imaginary part $\Im f(t)$ (defined in Eq.6.15) for optimized gates with m frequencies with $m = 2, 3, 6$, shown in $(a), (b), (c)$ respectively (depicted in color changing from blue to red). The corresponding trajectories for gates induced by monochromatic driving are depicted in black (the black trajectories are executed m times).

is based on a displacement of the bus mode in phase space conditioned on the state of the qubit degrees of freedom, where the displacement is encoded by the real and imaginary part of the function $f(t)$ as following

$$\mathcal{U}_{\mathcal{K}} = \exp\left(-i\big((\Re f(t)x + \Im f(t)p)\mathcal{S}_x - g(t)\mathcal{S}_x^2\big)\right) . \tag{6.15}$$

Here $x = a + a^\dagger$ and $p = i(a - a^\dagger)$ are the operator valued part of position and momentum of the bus mode.

The real part $\Re f(t)$ and imaginary part $\Im f(t)$ are depicted in Fig. (6.8) for optimized gates with $m = 2, 3$ and 6 frequencies. The color ranging from blue to red indicates evolving time where blue colour corresponds to the beginning of the gate and red corresponds to the end of the gate. The phase-space trajectory corresponding to the conventional gate is a circu-

lar orbit around a point positioned with a finite displacement with respect to the origin of the plane. In contrast, the trajectory corresponding to the polychromatic gate is a closed orbit forming excursions around the origin of the plane, and as m [2] tends to infinity, the trajectory tends to form perfect circles centred around the origin, and eventually the radii for the conventional and polychromatically driven gates coincide. Furthermore, the main difference between the two trajectories is encoded in the realisation of the constraint $\mathfrak{F}\{f;\bullet\} = 0$, which generates this shift of displacement from a finite point to the origin of the phase-space. On the other hand, the satisfaction of this constraint has a substantial impact on the functional $\mathfrak{F}\{ff^*;\bullet\} = 0$ which reads

$$\mathfrak{F}\{ff^*;\mathbb{I}\} = \sum_{j=1}^{m} \frac{c_j c_j^*}{j^2} + \sum_{j,k=1}^{m} \frac{c_j c_k^*}{jk}. \tag{6.16}$$

As one can see the second term is equal to the norm of the functional $|\mathfrak{F}\{f;\mathbb{I}\}|^2$, which is already suppressed for the optimised gate and the first term reduces to $\lambda_1/16$ defined via Eq. 6.13, and as m tends to infinity, λ_1 tends to $1/m$, and eventually the optimised quantity becomes $1/(16m)$. For the conventional gate however, the second term in the summation does not vanish and for the Rabi frequency $\eta\Omega = 1/(4\sqrt{m})$ the whole summation becomes $1/(8m)$ which is twice the magnitude for the polychromatic gate. So the asymptotic magnitude of the improvement R is 2 as can be foreseen from Fig.(6.3).

So far we have been examining the performance of the entangling operation from the gate-infidelity perspective. That is, the obtained evaluations were based on the 2-norm of the approximate error channel *i.e.* $\| \Xi[\circ] \|_2$ without any direct reference to the underlying density operator $\tilde{\varrho}$. Here we would like to assess the gate performance in terms of the measure of the information entropy corresponding to the underlying density operator for a two-qubit system. In the following we evaluate the achievable entangle-

[2] For finite m circles are not perfect, but their radii change with time.

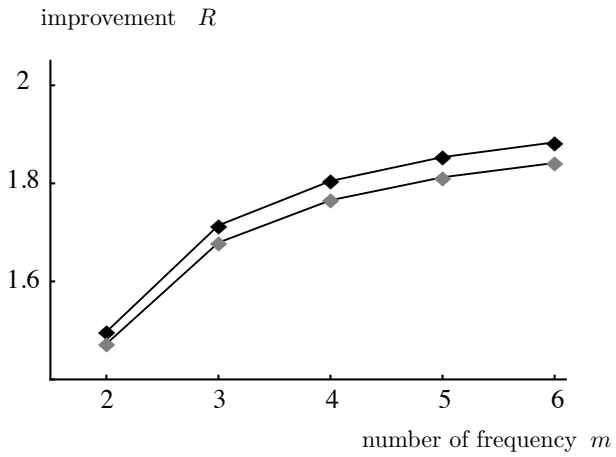

Figure 6.5: Improvement R_E of the deviation of EoF from its ideal value of 1 in terms of the number of frequencies of an optimal polychromatic pulse for a two-qubit gate, $N = 2$. All data correspond to $\gamma_- = \gamma_+ > 0, \gamma_d = 0$, with $\gamma_- = 10^{-3}\delta$ depicted in solid and, $\gamma_- = 10^{-2}\delta$ depicted in grey diamonds.

ment of a two-qubit gate in terms of entanglement of formation (EoF), E [56] based on a numerically exact simulation of the gate dynamics, and this extends the applicability of the assessment of the gate performance to the regime of strong dissipations. EoF is defined as

$$E(\varrho) = \mathfrak{E}[C(\varrho)] \qquad \text{with} \qquad C(\varrho) = \max\{0, \lambda_1 - \lambda_2 - \lambda_3 - \lambda_4\} \quad (6.17)$$

where the concurrence C is defined in terms of the eigenvalues in decreasing order of the density matrix $\sqrt{\sqrt{\varrho}\bar{\varrho}\sqrt{\varrho}}$ with $\bar{\varrho} = (\sigma_y \otimes \sigma_y)\varrho^*(\sigma_y \otimes \sigma_y)$. The function $\mathfrak{C}$ reads

$$\begin{aligned} \mathfrak{E}[u] &= h\Big(\frac{1+\sqrt{1-u^2}}{2}\Big) \qquad \text{with} \\ h(u) &= -u\log_2 u - (1-u)\log_2(1-u). \end{aligned}$$

Fig.(6.5) depicts the ratio $R_E = (1 - E_m)/(1 - E_p)$ of the deviation of EoF from 1 for a monochromatic and an optimized polychromatic two-qubit

gate, where E_m and E_p denote EoF for the monochromatic and polychromatic gate respectively. One can see that similarly to Fig.(6.3), already pulses with $m = 2$ frequencies yield a substantial improvement, and the improvement increases to a factor of 1.9 for pulse with $m = 6$ frequencies in the regime of weak dissipation as depicted by solid diamonds. Significantly, the improvement is not limited to the regime of weak dissipation, and as depicted by grey diamonds, by increasing the dissipative rates by an order of magnitude, the optimised pulse still yields a substantial improvement.The consistency of the obtained result with respect to the figure (6.3) shows that the operator norm of the dynamical map is an accurate figure of merit in characterising the entangling gate infidelity.

6.2.2 Dephasing

Now let us consider the case where there is an additional predominant process, namely dephasing which is phenomenologically described in terms of the operator $\tilde{E}_d$. The exact form of the ζ-matrix is provided in the appendix, but here we will suffice to read off the error channel which consists of the infinitesimal dissipative processes as following

$$\begin{aligned}\Xi[\circ] \quad : \quad & (\mathfrak{F}\{f + fff^*; a\} + \mathfrak{F}\{f^* + ff^*f^*; a^\dagger\})(-i[\xi_1, \circ]), \mathfrak{F}\{ff^*; \hat{n}\}\mathcal{D}_{\xi_1}[\circ], \\ & \mathfrak{F}\{fff^*f^*; \mathbb{I}\}\mathcal{D}_{\xi_2}[\circ], (\mathfrak{F}\{fff^*; a\} + \mathfrak{F}\{ff^*f^*; a^\dagger\})\mathcal{D}_{\xi_1+\xi_2}[\circ]. \end{aligned} \tag{6.18}$$

The optimisation procedure is same as in the case where thermalisation was the only dissipative process in the system except that here we should include the extra constraint $\mathfrak{F}\{fff^*; \bullet\} = 0$. Fig.(6.7) depicts the amplitudes corresponding the highest frequency component of the optimised pulse in comparison with the pulse amplitudes optimised in the presence of thermalisation only; the exemplary cases for optimised pulses with $m = 8$ [3] is depicted in Fig.(6.7).

[3]The minimum number of frequencies satisfying the optimization condition imposed by the constraints is $m = 3$.

Similar to the case of thermalisation, as the index j of the driving frequency $j\omega$ with $j = 1, ..., m$ increases, the absolute magnitudes of the corresponding driving amplitudes grows, and this pattern is totally independent of the number of driving frequencies m. In contrast to the case of thermalisation, amplitudes corresponding to the lowest and the highest frequency components are phase-shifted by π with respect to all the other amplitudes.

The real part $\Re f(t)$ and imaginary part $\Im f(t)$ are depicted in Fig. (6.8) for optimized gate with $m = 3, 4$ and 7 frequencies. The phase space trajectories for the corresponding monochromatic case, as depicted in black, describes circular motion around a phase space point of finite displacement from the origin. In the polychromatic case on the other hand, the trajectory circulates with a zero-averaged displacement which is imposed by the constraint $\mathfrak{F}\{f + fff^*; \bullet\} = 0$. As the number of frequencies m increase, the trajectory is approximated better and better by circles around the origin.

Fig.(6.9) depicts the improvement R defined in terms of the ratio of the gate infidelities $\mathcal{I}$ for an optimized pulse and a monochromatic pulse, $\mathcal{I}_m/\mathcal{I}_p$ in a two-qubit system $(N = 2)$ with an environment model for which ($\gamma_+ = \gamma_- = 0 = \gamma_d > 0$, where the rates γ_+, γ_- and γ_d are defined in Eq.(6.3)). Empty (full) circles correspond to the improvement induced by the polychromatic pulse $\Upsilon_p(t)$ which is optimised with respect to the constraints $\mathfrak{F}\{f + fff^*; \bullet\} = 0$ $(\mathfrak{F}\{f\}; \bullet\} = 0)$. The bus mode is assumed to be in its ground state. As one can see, a pulse with three frequencies which permits to realize the conditions $\mathfrak{F}\{f + fff^*; \bullet\} = 0$, yields an improvement by a factor around 1.7, and by incorporating higher number of frequencies we observe further improvement in the suppression of the induced infidelity as the rate R asymptotes to the value of 2. Unlike the case of thermalisation, the gate improvement depends on the bus mode excitation $\langle\hat{n}\rangle$, as the inset depicts the dependence of R on the mean phonon excitation $\langle\hat{n}\rangle$. In this exemplary case of $m = 5$, there is a slight drop of improvement with increasing $\langle\hat{n}\rangle$, but even in the limit of large excitations,

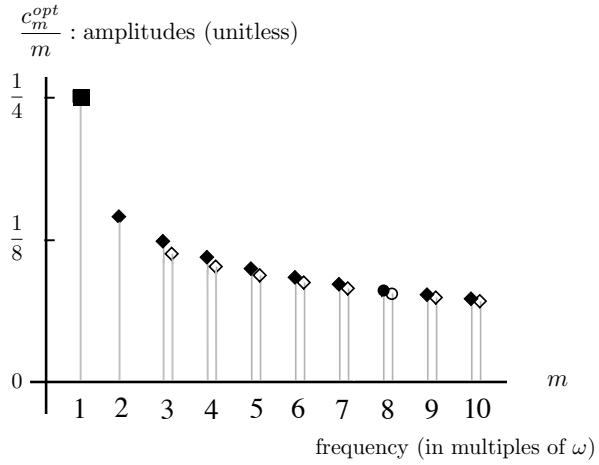

Figure 6.6: The filled square depicts the amplitude for a monochromatic pulse and the filled (empty) diamonds depict the amplitude of the highest frequency component c_m^{opt}/m optimised with one (two) constraints, with m ranging from $2(3)$ to 10

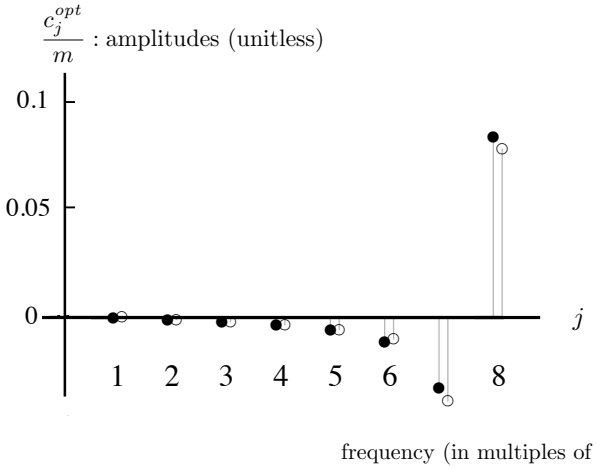

Figure 6.7: The filled (empty) circles depict the amplitudes c_j^{opt}/m of the optimal pulse (Eq.(6.12)) with one (two) constraints for $m = 8$ frequency components. The amplitude of the highest frequency component is always dominant and phase shifted as compared to all (almost all) other amplitudes.

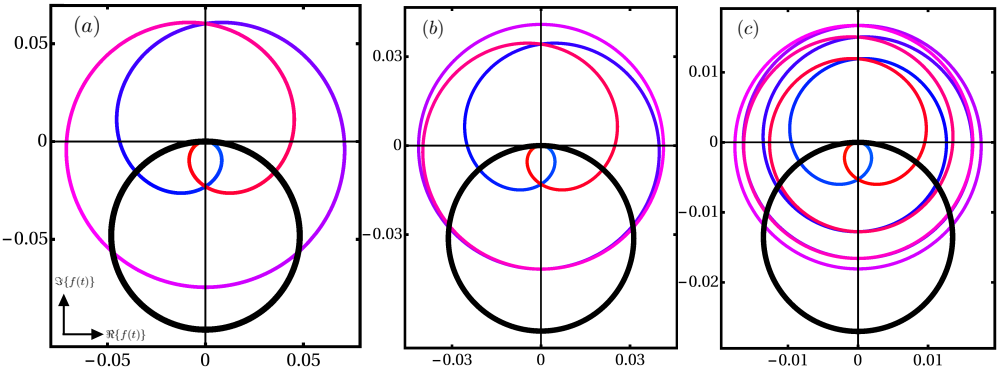

Figure 6.8: Phase-space trajectories of the bus mode characterized by $\Re f(t)$ and imaginary part $\Im f(t)$ (defined in Eq.6.15) for optimized gate with $m = 3, 4$ and 7 frequencies (depicted in color changing from blue to red). The corresponding trajectory for gate induced by monochromatic driving is depicted in black (the black trajectory is executed m times).

improvements around 1.85 are reached.

As one can see pulse optimised with one constraint $\mathfrak{F}\{f;\bullet\} = 0$ yields slightly better improvement in the gate performance compared with the pulse which is optimised with the additional constraint $\mathfrak{F}\{fff^*;\bullet\} = 0$ as the second significant component of the optimal control is the minimisation of $\mathfrak{F}\{ff^*;\bullet\}$, that is we observe better suppression of induced infidelity with the minimization of $\mathfrak{F}\{ff^*;\bullet\}$ under the constraint $\mathfrak{F}\{f;\bullet\} = 0$ rather than the two constrains $\mathfrak{F}\{f + fff^*;\bullet\} = 0$. Furthermore, the optimal pulse $\Upsilon(t)$ obtained in this fashion typically coincides with solutions which minimize the functional $\mathfrak{F}\{fff^*f^*;\bullet\}$, and therefore we obtain driving patterns that optimise the gate performance independently of the bus mode properties.

Fig.(6.10) depicts the ratio $R_E = (1 - E_m)/(1 - E_p)$ of the deviation

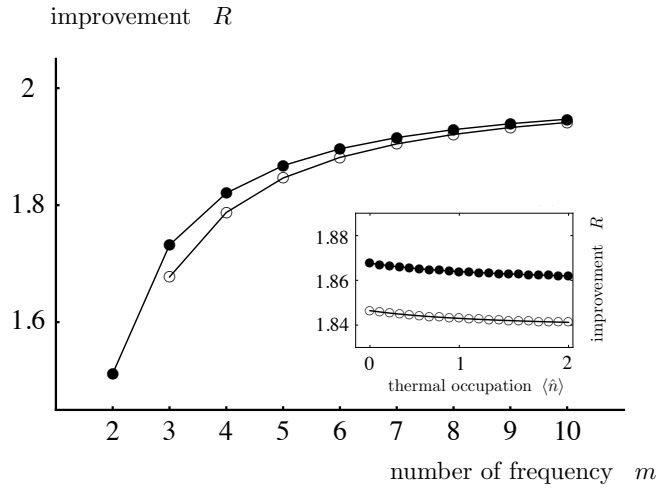

Figure 6.9: Improvement R in terms of the number of frequencies of an optimal polychromatic pulse for a two-qubit gate, $N = 2$ which is subject to thermalisation and dephasing. Filled circles correspond to the pulse optimised with the constraint $\mathfrak{F}\{f; \bullet\} = 0$, and empty circles correspond to the pulse optimised with the additional constraint $\mathfrak{F}\{fff^*; \bullet\} = 0$. The inset depicts the dependence of the improvement R on the excitation $\langle \hat{n} \rangle$ for a thermal state of the bus mode and a pulse of $m = 5$ frequencies.

of EoF from 1 for a monochromatic and an optimized polychromatic two-qubit gate, where E_m and E_p denote EoF for the monochromatic and polychromatic gate respectively. One can see that similarly to Fig.(6.9), already pulses with $m = 3$ frequencies yield a substantial improvement, and the improvement increases to nearly a factor of 2 for pulse with $m = 7$ frequencies in the regime of weak dissipation as depicted by black diamonds. Even in the regime of strong dissipations we observe substantial improvement in the suppression of the gate infidelity.

Only for an environment model that does not contain any pure dephasing (*i.e.* $\gamma_d = 0$), the improvement R is indeed independent of the number of ions. In contrast, as the additional dephasing process is introduced to

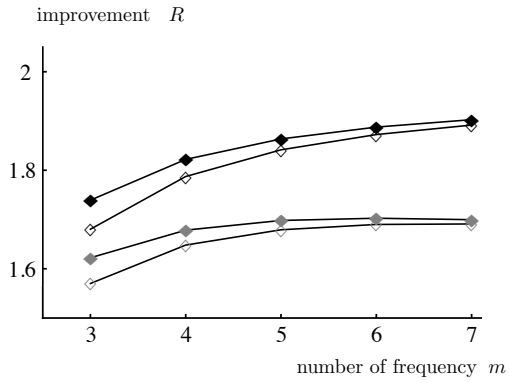

Figure 6.10: Filled (empty) diamonds depict the improvement R_E of the entanglement of formation (EoF) from its ideal value of 1 for the polychromatic pulse optimized with one (two) constraint(s) in terms of the number of frequencies for a two-qubit gate, $N = 2$. All data correspond to $\gamma_- = \gamma_+ = \gamma_d > 0$, with $\gamma_d = 10^{-3}\delta$ depicted in solid and, $\gamma_d = 10^{-2}\delta$ depicted in grey diamonds.

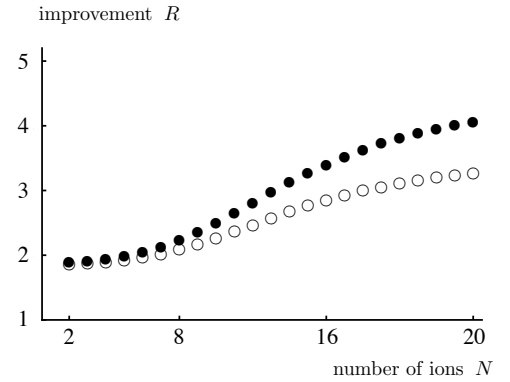

Figure 6.11: Improvement R as function of the number of ions for a pulse with $m = 3(7)$ frequencies depicted by circle(diamond) symbols corresponding to the environment model $\gamma_+ = \gamma_- = 0$, $\gamma_d > 0$. The improvement rapidly grows with N and the asymptotic improvement (for $N \to \infty$) grows with m.

the system, improvement in gate performance becomes highly dependent on the number of ions, and in fact, as Fig. 6.11 shows, this improvement grows with the number of ions. For a pulse with 6 frequencies R reaches values exceeding 4. Although even in the absence of dephasing, the gate performance is dependent on the number of ions, it is the ratio of infidelities R which does not depend on N. In the presence of dephasing however, N does not factor out in the calculation of R, which itself is expressed in terms of the coefficient matrix ζ. As we have discussed in Sec. C.1, the rates at which the collective phase-flips of four ions induced by dephasing of the bus mode takes place, scale with N^4. Since most of these processes are suppressed for optimized pulses due to the constraint $\mathfrak{F}\{f;\bullet\} = 0$, and the remaining contributions are being minimized, the improvement indeed grows with N.

Chapter 7

Conclusion

In this thesis we have presented a theoretical analysis on the behaviour of driven open quantum systems. The core result of our research consists of the development of a mathematical method by which valid approximations to the dynamics of driven open quantum systems with time-dependant generators, can be constructed, and the development of an optimisation method by which the dynamics of quantum gates based on the system of trapped ions that are subject to irreversible processes, can be manipulated and controlled. By applying the proposed schemes to several physical dissipative systems including two-level systems, harmonic oscillators, and three-level systems, and assessing their conduct using numerical simulations, our methods have proven to be a significant step towards the optimal control and simulation of open quantum systems.

In chapter 5, we proposed a matrix correction scheme based on which the non-positive coefficient matrix corresponding to the truncated effective generator of a driven open system, is replaced with a corrected, positive semidefinite matrix. By applying this correction scheme to several driven fundamental quantum systems including two-level systems, harmonic oscillators, and three-level systems, we have demonstrated that not only the fundamental property of positivity of the induced dynamics is ensured, but also the accuracy to which it approximates the exact dynamics is sig-

nificantly improved.

A mathematical method which permits to construct valid approximations to the exact dynamics of driven open quantum systems, can be a promising tool in designing effective irreversible processes. Alternatively, the proposed scheme permits to design effective generators at any order of the approximation encoding effective dissipative processes. From this perspective our correction method opens new possibilities in the domain of optimal control, and simulation of irreversible quantum dynamics.

In the domain of variational analyses in which one is interested in the optimisation of a specific aspect of a quantum system, for example the preparation of a desired state or the implementation of a quantum gate, the validity of the approximated map becomes quite crucial. If the variation of the variable over which the value of figure of merit (target functional) is optimised at the same time results in a reduced accuracy of the employed approximation, there will be no insurance that the optimised control variables would generate the desired dynamics, but a model which installs the system's fundamental structure on the utilised approximations, will likely limit such deviations.

In chapter 6, we presented an analysis on the dynamics of MS entangling gate in the presence of motional decoherence. By proposing a polychromatic implementation of the scheme, and by applying mathematical optimisation techniques, we were able to construct optimally shaped pulses independently of the environment model *e.g.* decoherence rate or thermal occupation. By comparing the infidelity of the polychromatically driven optimised gate with the conventional implementation, we observed a significant improvement in the performance of the former. Furthermore, by utilising our optimally obtained pulses in gates with large number of ions, we assessed a substantial enhancement in the gate performance compared with gates with only two ions.

Since the limitations in the obtained fidelities of multi-qubit entangling gates pose an obstacle in reaching fault tolerance, the increased robustness

with respect to motional decoherence promises to advance control over trapped ions substantially, which paves the way to the realisation of the true potential of quantum mode of computation *e.g.* solving mathematical problems that are considered intractable on a classical Turing machine. In the modern implementation of ions traps, which is based on surface electrode architecture, the string of ions are positioned near noisy trap electrodes [57–60], such that the bus mode of the ions is subject to severe heating processes, and this is a major challenge which is hard to overcome. As we have shown, the gate infidelities induced by finite motional noise levels can be suppressed substantially, and this can be a significant step towards controlling the decoherence, and eventually being able to suppress the noise level in modern surface electrode traps considerably.

The observed improvement in the fidelity of gates involving many ions also offers an interesting possibility in the deconstruction of quantum algorithm into individual gates. As our work indicates, rather than decomposing an algorithm into individually optimised single and two-qubit gates, one might obtain substantially better performance by incorporating also optimised three-qubit gates (such as the Toffoli gate) or even gates involving more than just two qubits. In situations in which N-qubit gates are realizable (such as trapped ions), apart from a correspondingly reduced number of elementary gates, the increased improvement through control that three-(or more) qubit gates offer would be advantageous.

Bibliography

[1] S. Lloyd, Science **273**, 1073 (1996).

[2] J. I. Cirac and P. Zoller, Phys. Rev. Lett. **74**, 4091 (1995).

[3] A. Sørensen and K. Mølmer, Phys. Rev. Lett. **82**, 1971 (1999).

[4] W. Magnus, Commun.Pure Appl.Math. **7**, 649 (1954).

[5] F. J. Dyson, Phys. Rev. **75**, 486 (1949).

[6] J. T. Barreiro, M. Müller, P. Schindler, D. Nigg, T. Monz, M. Chwalla, M. Hennrich, C. F. Roos, P. Zoller, and R. Blatt, Nature **470**, 486 (2011).

[7] K. Mølmer and A. Sørensen, Phys. Rev. Lett. **82**, 1835 (1999).

[8] H. Häffner, W. Hänsel, C. Roos, J. Benhelm, M. Chwalla, T. Körber, U. Rapol, M. Riebe, P. Schmidt, C. Becher, O. Gühner, W. Dür, and R. Blatt, Nature **438**, 643 (2005).

[9] R. Blatt and D. Wineland, Nature **453**, 1008 (2008).

[10] F. Schmidt-Kaler, H. Häffner, M. Riebe, S. Gulde, G. P. Lancaster, T. Deuschle, C. Becher, C. F. Roos, J. Eschner, and R. Blatt, Nature **422**, 408 (2003).

[11] C. Sackett, D. Kielpinski, B. King, C. Langer, V. Meyer, C. Myatt, M. Rowe, Q. Turchette, W. Itano, D. Wineland, and C. Monroe, Nature **404**, 256 (2000).

[12] A. Politi, J. C. Matthews, and J. L. O'Brien, Science **325**, 1221 (2009).

[13] B. P. Lanyon, C. Hempel, D. Nigg, M. Müller, R. Gerritsma, F. Zähringer, P. Schindler, J. T. Barreiro, M. Rambach, G. Kirchmair, M. Hennrich, P. Zoller, R. Blatt, and C. F. Roos, Science **334**, 57 (2011).

[14] M. Riebe, H. Häffner, C. Roos, W. Hänsel, J. Benhelm, G. Lancaster, T. Körber, C. Becher, F. Schmidt-Kaler, D. James, and R. Blatt, Nature **429**, 734 (2004).

[15] M. Barrett, J. Chiaverini, T. Schaetz, J. Britton, W. Itano, J. Jost, E. Knill, C. Langer, D. Leibfried, R. Ozeri, and D. J. Wineland, Nature **429**, 737 (2004).

[16] V. Giovannetti, S. Lloyd, and L. Maccone, Science **306**, 1330 (2004).

[17] T. P. Harty, D. T. C. Allcock, C. J. Ballance, L. Guidoni, H. A. Janacek, N. M. Linke, D. N. Stacey, and D. M. Lucas, Phys. Rev. Lett. **113**, 220501 (2014).

[18] C. J. Ballance, T. P. Harty, N. M. Linke, M. A. Sepiol, and D. M. Lucas, Phys. Rev. Lett. **117**, 060504 (2016).

[19] N. Timoney, I. Baumgart, M. Johanning, A. Varón, M. Plenio, A. Retzker, and C. Wunderlich, Nature **476**, 185 (2011).

[20] T. R. Tan, J. P. Gaebler, R. Bowler, Y. Lin, J. D. Jost, D. Leibfried, and D. J. Wineland, Phys. Rev. Lett. **110**, 263002 (2013).

[21] D. Leibfried, B. DeMarco, V. Meyer, D. Lucas, M. Barrett, J. Britton, W. Itano, B. Jelenković, C. Langer, T. Rosenband, and D. J. Wineland, Nature **422**, 412 (2003).

[22] T. Monz, P. Schindler, J. T. Barreiro, M. Chwalla, D. Nigg, W. A. Coish, M. Harlander, W. Hänsel, M. Hennrich, and R. Blatt, Phys. Rev. Lett. **106**, 130506 (2011).

[23] H. M. Wiseman and G. J. Milburn, *Quantum measurement and control* (Cambridge University Press, 2009).

[24] H.-P. Breuer and F. Petruccione, *The theory of open quantum systems* (Oxford University Press, 2002).

[25] G. Lindblad, Commun. Math. Phys. **48**, 119 (1976).

[26] R. Ingarden and A. Kossakowski, Ann. Phys **89**, 451 (1975).

[27] R. Bhatia, *Matrix analysis*, Vol. 169 (Springer Science & Business Media, 2013).

[28] W. F. Stinespring, Proc. Amer. Math. Soc. **6**, 211 (1955).

[29] M.-D. Choi, Linear algebra and its applications **10**, 285 (1975).

[30] R. Alicki, in *Quantum Dynamical Semigroups and Applications* (Springer, 1987) pp. 1–94.

[31] R. Blatt and C. Roos, Nat. Phys. **8**, 277 (2012).

[32] C. Cohen-Tannoudji, J. Dupont-Roc, G. Grynberg, and P. Thickstun, *Atom-photon interactions: basic processes and applications* (Wiley Online Library, 1992).

[33] S. Rahav, I. Gilary, and S. Fishman, Phys. Rev. A **68**, 013820 (2003).

[34] A. Verdeny, A. Mielke, and F. Mintert, Phys. Rev. Lett. **111**, 175301 (2013).

[35] N. Goldman and J. Dalibard, Phys. Rev. X **4**, 031027 (2014).

[36] S. Weinberg, *The quantum theory of fields*, Vol. 1 (Cambridge university press, 1995).

[37] D. A. Lidar and T. A. Brun, *Quantum error correction* (Cambridge University Press, 2013).

[38] A. Iserles and S. Norsett, Philoc. Trans. R. Soc. London, Ser. A , 983 (1999).

[39] S. Blanes, F. Casas, J. Oteo, and J. Ros, Physics Reports **470**, 151 (2009).

[40] D. Kielpinski, C. Monroe, and D. J. Wineland, Nature **417**, 709 (2002).

[41] D. Leibfried, R. Blatt, C. Monroe, and D. Wineland, Rev. Mod. Phys. **75**, 281 (2003).

[42] M. A. Nielsen and I. L. Chuang, *Quantum computation and quantum information* (Cambridge university press, 2010).

[43] D. Deutsch, in *Proc. R. Soc. London A*, Vol. 425 (The Royal Society, 1989) pp. 73–90.

[44] M. M. Wolf and J. I. Cirac, Commun. Math. Phys. **279**, 147 (2008).

[45] D. Evans and L. John, Comm. Dublin Inst. Adv. Studies, Ser. A **24**, 104 (1977).

[46] R. A. Horn and C. R. Johnson, *Matrix analysis* (Cambridge university press, 2012).

[47] S. Kohler, T. Dittrich, and P. Hänggi, Phys. Rev. E **55**, 300 (1997).

[48] M. Schlosshauer, A. P. Hines, and G. J. Milburn, Phys. Rev. A **77**, 022111 (2008).

[49] T.-P. Cheng, L.-F. Li, and T.-P. Cheng, *Gauge theory of elementary particle physics* (Clarendon press Oxford, 1984).

[50] J. Benhelm, G. Kirchmair, C. F. Roos, and R. Blatt, Nat. Phys. **4**, 463 (2008).

[51] G. Kirchmair, J. Benhelm, F. Zähringer, R. Gerritsma, C. Roos, and R. Blatt, New. J. Phy. **11**, 023002 (2009).

[52] D. Hayes, S. M. Clark, S. Debnath, D. Hucul, I. V. Inlek, K. W. Lee, Q. Quraishi, and C. Monroe, Phys. Rev. Lett. **109**, 020503 (2012).

[53] A. Sørensen and K. Mølmer, Phys. Rev. A **62**, 022311 (2000).

[54] A. Gilchrist, N. K. Langford, and M. A. Nielsen, Phys. Rev. A **71**, 062310 (2005).

[55] A. Verdeny, L. Rudnicki, C. A. Müller, and F. Mintert, Phys. Rev. Lett. **113**, 010501 (2014).

[56] W. K. Wootters, Phys. Rev. Lett. **80**, 2245 (1998).

[57] J. Labaziewicz, Y. Ge, D. R. Leibrandt, S. X. Wang, R. Shewmon, and I. L. Chuang, Phys. Rev. Lett. **101**, 180602 (2008).

[58] J. Labaziewicz, Y. Ge, P. Antohi, D. Leibrandt, K. R. Brown, and I. L. Chuang, Phys. Rev. Lett. **100**, 013001 (2008).

[59] C. Ospelkaus, U. Warring, Y. Colombe, K. Brown, J. Amini, D. Leibfried, and D. Wineland, Nature **476**, 181 (2011).

[60] A. Safavi-Naini, P. Rabl, P. F. Weck, and H. R. Sadeghpour, Phys. Rev. A **84**, 023412 (2011).

Appendices

Appendix A

In this section, we provide details for the general construction of effective generators, and the interpretation of such generators in terms of effective processes for the driven two-level system and the driven harmonic oscillator.

A.1 Derivation of effective generators

The series expansion

$$\mathcal{L}_n = \sum_{m=0}^{n} \frac{\mathcal{A}^{(m)}}{\omega^m}$$

of the generator is characterized by the (super-)operators $\mathcal{A}^{(m)}$. They read [35]

$$\begin{aligned}
\mathcal{A}^{(0)} &= \tilde{\mathcal{L}}_0 \\
\mathcal{A}^{(1)} &= \sum_{\nu=1}^{\infty} \frac{i}{\nu}[\tilde{\mathcal{L}}_\nu, \tilde{\mathcal{L}}_{-\nu}] + \sum_{\nu=1}^{\infty} \frac{i}{\nu}[\tilde{\mathcal{L}}_0, \tilde{\mathcal{L}}_\nu - \tilde{\mathcal{L}}_{-\nu}] \\
\mathcal{A}^{(2)} &= \sum_{\nu,\mu\neq 0}^{\infty} \frac{1}{2\nu\mu}[[\tilde{\mathcal{L}}_\nu, \tilde{\mathcal{L}}_{-\nu}], \tilde{\mathcal{L}}_\mu] - \sum_{\nu\neq\mu\neq 0}^{\infty} \frac{1}{2\nu\mu}[\tilde{\mathcal{L}}_\nu, [\tilde{\mathcal{L}}_0, \tilde{\mathcal{L}}_\mu]] \\
&- \sum_{\nu,\mu\neq 0}^{\infty} \frac{1}{3\nu\mu}[\tilde{\mathcal{L}}_\nu, [\tilde{\mathcal{L}}_\mu, \tilde{\mathcal{L}}_{-\nu-\mu}]] + \sum_{\nu\neq 0}^{\infty} \frac{1}{2\nu^2}[\tilde{\mathcal{L}}_0, [\tilde{\mathcal{L}}_0, \tilde{\mathcal{L}}_\nu]] \\
&+ \sum_{\nu=1}^{\infty} \sum_{\substack{\mu\neq 0 \\ \mu\neq -\nu}} \frac{1}{2\nu(\nu+\mu)}[[\tilde{\mathcal{L}}_\nu, \tilde{\mathcal{L}}_\mu] + [\tilde{\mathcal{L}}_{-\nu}, \tilde{\mathcal{L}}_{-\mu}], \tilde{\mathcal{L}}_0]
\end{aligned}$$

in terms of the Fourier coefficients

$$\tilde{\mathcal{L}}_\nu = \frac{1}{T}\int_0^T dt\ \mathcal{L}_t e^{-i\nu\omega t}$$

of the time-dependent generator $\mathcal{L}_t$.

For any given operator basis E_p, the operators $\mathcal{A}^{(m)}$ can be expressed as

$$\mathcal{A}^{(m)}(\circ) = \sum_{p,q=0}^{d^2-1} \alpha_{pq}^{(m)} E_p \circ E_q^\dagger \ ,$$

where d is the dimension of the Hilbert space of the system. It is convenient to choose E_0 to be the identity id. With this choice, the m^{th}-order contribution to the effective Hamiltonian reads

$$H^{(m)} = \frac{i}{2}\sum_{p=1}^{d^2-1} (\alpha_{p0}^{(m)} E_p - (\alpha_{p0}^{(m)})^* E_p^\dagger) \ .$$

Since the dynamics is trace-preserving, any $\mathcal{A}^{(m)}$ necessarily satisfies $\mathrm{Tr}\mathcal{A}^{(m)}\circ =$

0, what implies

$$\alpha_{00}^{(m)} + \sum_{p=1}^{d^2-1} \alpha_{p0}^{(m)} E_p + \sum_{p=1}^{d^2-1} \alpha_{0p}^{(m)} E_p^\dagger + \sum_{p,q=1}^{d^2-1} \alpha_{pq}^{(m)} E_q^\dagger E_p = 0 \; .$$

This, in turn, allows to express $\mathcal{A}^{(m)}$ as

$$\begin{aligned} \mathcal{A}^{(m)}(\circ) &= -i[H^{(m)}, \circ] \\ &+ \sum_{p,q=1}^{d^2-1} \mathbf{D}_{pq}^{(m)} \left(E_p \circ E_q^\dagger - \frac{1}{2}\{E_q^\dagger E_p, \circ\} \right) \end{aligned} \tag{1}$$

with the Hermitian operator $H^{(m)}$ and the coefficient matrix $\mathbf{D}^{(m)}$ with elements

$$\mathbf{D}_{pq}^{(m)} = \alpha_{pq}^{(m)} \text{ for } p, q = 1, \ldots, d^2 - 1 \; .$$

This, finally yields the effective generator

$$\mathcal{L}_n(\circ) = -i[\mathcal{H}_n, \circ] + \sum_{p,q=1}^{d^2-1} [\mathcal{C}_n]_{pq} (E_p \circ E_q^\dagger - \frac{1}{2}\{E_q^\dagger E_p, \circ\})$$

in terms of the effective Hamiltonian $\mathcal{H}_n = \sum_{m=0}^{n} \frac{H^{(m)}}{\omega^m}$ and the effective coefficient matrix $\mathcal{C}_n = \sum_{m=0}^{n} \frac{\mathbf{D}^{(m)}}{\omega^m}$.

A.2 Phenomenological description of the effective processes

For the physical interpretation of the processes described by the dissipator

$$\mathcal{Z}[\circ] = \sum_{pq} [\tilde{\mathcal{C}}_n]_{pq} (E_p \circ E_q^\dagger - \frac{1}{2}\{E_q^\dagger E_p, \circ\})$$

it is helpful to define operators

$$F_p = \sum_q U_{pq} E_p \tag{2}$$

in terms of the unitary transformation U that diagonalizes $\tilde{\mathcal{C}}_n$. With the eigenvalues $\tilde{\lambda}_i^{(n)}$ of $\tilde{\mathcal{C}}_n$ the above dissipator reads

$$\mathcal{Z}[\circ] = \sum_i \tilde{\lambda}_i^{(n)} (F_i \circ F_i^\dagger - \frac{1}{2}\{F_i^\dagger F_i, \circ\})$$

and $\tilde{\lambda}_i^{(n)}$ can be interpreted as the rate for the process described by the operator F_i Ref. [24].

A.2.1 Driven two-level system

The effective Hamiltonian of the driven two-level system (including second order contributions) is diagonalized by

$$\mathcal{U}_\mathcal{H} = \exp\left(\frac{i}{\omega}\left(\Omega_s \sigma_x + \Omega_c \left(\frac{\omega_0}{\omega} - 4\frac{\gamma^2}{\omega\omega_0}\right)\sigma_y\right)\right) .$$

In terms of the rotated Pauli matrices

$$\tilde{\sigma}_i = \mathcal{U}_\mathcal{H} \sigma_i \mathcal{U}_\mathcal{H}^\dagger$$

the effective dissipator in the second order reads

$$\mathcal{Z}_2[\circ] = \sum_{p,q=1}^{3} \tilde{\mathcal{C}}_{pq} \left(\tilde{\sigma}_p \circ \tilde{\sigma}_q - \frac{1}{2}\{\tilde{\sigma}_q \tilde{\sigma}_p, \circ\}\right)$$

with the coefficient matrix

$$\tilde{\mathcal{C}} = \gamma \begin{bmatrix} 0 & 0 & 0 \\ 0 & 0 & 0 \\ 0 & 0 & 1 \end{bmatrix} + \gamma\eta \begin{bmatrix} 0 & 0 & 0 \\ 0 & 1 & 0 \\ 0 & 0 & -2 \end{bmatrix} + \gamma\zeta \begin{bmatrix} 0 & 0 & 1 \\ 0 & 0 & 0 \\ 1 & 0 & 0 \end{bmatrix} .$$

with $\eta = \gamma(\Omega_s^2 + \Omega_c^2)/\omega^2$ and $\zeta = \frac{\Omega_c}{\omega_0\omega^2}(6\omega_0^2 - 8\gamma^2)$. In first order approximation $\tilde{\mathcal{C}}$ is diagonal and γ is the only non-vanishing eigenvalue. That is, the effective dissipator $\mathcal{Z}_1$ reads

$$\mathcal{Z}_1 = \gamma\mathcal{D}_{\tilde{\sigma}_z} ,$$

and describes dephasing in the eigenbasis of $\tilde{\sigma}_z$, *i.e.* the eigenbasis of the effective Hamiltonian.

In second order approximation $\tilde{\mathcal{C}}$ is no longer diagonal, but the diagonalization is achieved with the unitary matrix

$$\tilde{U} = e^{-i\zeta\hat{S}_y} ,$$

with

$$\hat{S}_y = \begin{bmatrix} 0 & 0 & -i \\ 0 & 0 & 0 \\ i & 0 & 0 \end{bmatrix} .$$

In terms of the operators

$$\begin{aligned} \sigma'_x = \sum_i \tilde{U}_{xi}\tilde{\sigma}_i &= \cos(\zeta)\tilde{\sigma}_x - \sin(\zeta)\tilde{\sigma}_z \\ \sigma'_y = \sum_i \tilde{U}_{yi}\tilde{\sigma}_i &= \tilde{\sigma}_y \\ \sigma'_z = \sum_i \tilde{U}_{zi}\tilde{\sigma}_i &= \cos(\zeta)\tilde{\sigma}_z + \sin(\zeta)\tilde{\sigma}_x \end{aligned}$$

defined according to Eq. (2). With the corrected eigenvalues $\tilde{\lambda}_1 = \gamma(1-\eta)^2$

and $\tilde{\lambda}_2 = \gamma\eta$ the effective dissipator in second order then reads

$$\mathcal{Z}_2 = \gamma(1-\eta)^2\mathcal{D}_{\sigma_z'} + \gamma\eta\mathcal{D}_{\sigma_y'} \ ,$$

and it induces the two dephasing processes described in the main text.

A.2.2 Harmonic oscillator

The effective Hamiltonian $\mathcal{H}_2$ of the harmonic oscillator in second order approximation is diagonalized with the unitary transformation

$$\mathcal{U}_{\mathcal{H}} = e^{i\frac{\Omega}{\omega}(a+a^\dagger)} \ .$$

That is, the creation and annihilation operator for excitations of $\mathcal{H}_2$ read

$$\begin{aligned} \tilde{a} &= a - \frac{i\Omega}{\omega} \\ \tilde{a}^\dagger &= a^\dagger + \frac{i\Omega}{\omega} \end{aligned}$$

The coefficient matrix in terms of the operators $\tilde{a}$, $\tilde{a}^\dagger$ and

$$\tilde{n} = \tilde{a}^\dagger\tilde{a} = n + \frac{i\Omega}{\omega}(a - a^\dagger) + \frac{\Omega^2}{\omega^2} \tag{3}$$

reads

$$\tilde{\mathcal{C}} = \gamma \begin{bmatrix} 0 & 0 & 0 \\ 0 & 0 & 0 \\ 0 & 0 & 1 \end{bmatrix} - \frac{\gamma\Omega^2}{\omega^2} \begin{bmatrix} -1 & 1 & 0 \\ 1 & -1 & 0 \\ 0 & 0 & 1 \end{bmatrix}$$

Consequently, the effective dissipator in first order approximation reads

$$\mathcal{Z}_1 = \gamma\mathcal{D}_{\tilde{n}} \ ,$$

and it induces dephasing with rate γ in the eigenbasis of the effective Hamiltonian.

In second order approximation, there are two non-vanishing (renormalized) Lindblad operators that can be expressed as :

$$\begin{aligned} F_1 &= \tilde{n} + O(\omega^{-3}) \quad \text{and} \\ F_2 &= \tilde{p} + O(\omega^{-3}) \, , \end{aligned}$$

with the dimensionless momentum operator

$$\tilde{p} = \frac{i}{\sqrt{2}}(\tilde{a}^\dagger - \tilde{a})$$

in the frame defined by the effective Hamiltonian. The corresponding eigenvalues read

$$\begin{aligned} \lambda_1 &= \gamma(1 - \frac{\Omega^2}{\omega^2}) \quad \text{and} \\ \lambda_2 &= 4\gamma\frac{\Omega^2}{\omega^2} \ . \end{aligned}$$

With this, the effective dissipator reads

$$\mathcal{Z}_2 = \gamma \left(1 - \frac{\Omega^2}{2\omega^2}\right)^2 \mathcal{D}_{\tilde{n}} + 4\gamma\frac{\Omega^2}{\omega^2}\mathcal{D}_{\tilde{p}} \, ,$$

where the corrected transition rate $\tilde{\lambda}_1 = \gamma(1 - \frac{\Omega^2}{2\omega^2})^2$ is obtained by modifying the eigenvalue λ_1 following Eq.(2) in the main paper . In second order, the rate of dephasing is thus reduced by a factor of $(1 - \frac{\Omega^2}{2\omega^2})^2$, and, there is an additional process of diffusion in real space [16, 47] with rate $4\gamma\frac{\Omega^2}{\omega^2}$ described by the Lindblad operator $\tilde{p}$.

Appendix B

In this section we provide a brief description of the Gell-Mann matrices.

B.1 Gell-Mann matrices

Gell-Mann matrices are one of the possible representation of the generators of $SU(3)$ group. The underlying algebra of the generators obey the following commutation relation

$$[\mathscr{G}_i, \mathscr{G}_j] = i\mathscr{F}^{ijk} g_k \tag{4}$$

where the structure constant $\mathscr{F}^{ijk}$ is anti-symmetric in three indices wit the following values

$$\mathscr{F}^{123} = 1, \mathscr{F}^{147} = \mathscr{F}^{165} = \mathscr{F}^{246} = \mathscr{F}^{257} = \mathscr{F}^{345} = \mathscr{F}^{376} = \frac{1}{2}, \mathscr{F}^{458} = \mathscr{F}^{678} = \frac{\sqrt{3}}{2}$$

Gell-Mann matrices is a particular set of 3×3 traceless and self-conjugate matrix representation of these generators. They read as follwing

$$
\begin{aligned}
\mathscr{G}_1 &= \begin{bmatrix} 0 & 0 & 0 \\ 0 & 0 & 1 \\ 0 & 1 & 0 \end{bmatrix}, \ \mathscr{G}_2 = \begin{bmatrix} 0 & 0 & 0 \\ 0 & 0 & -i \\ 0 & i & 0 \end{bmatrix}, \ \mathscr{G}_3 = \begin{bmatrix} 0 & 0 & 0 \\ 0 & 1 & 0 \\ 0 & 0 & -1 \end{bmatrix}, \\
\mathscr{G}_4 &= \begin{bmatrix} 0 & 0 & 1 \\ 0 & 0 & 0 \\ 1 & 0 & 0 \end{bmatrix}, \ \mathscr{G}_5 = \begin{bmatrix} 0 & 0 & -i \\ 0 & 1 & 0 \\ i & 0 & 0 \end{bmatrix}, \\
\mathscr{G}_6 &= \begin{bmatrix} 0 & 1 & 0 \\ 1 & 0 & 0 \\ 0 & 0 & 0 \end{bmatrix}, \ \mathscr{G}_7 = \begin{bmatrix} 0 & -i & 0 \\ i & 0 & 0 \\ 0 & 0 & 0 \end{bmatrix}, \ \mathscr{G}_8 = \begin{bmatrix} 2 & 0 & 0 \\ 0 & -1 & 0 \\ 0 & 0 & -1 \end{bmatrix}. \quad (5)
\end{aligned}
$$

Appendix C

In this section we provide some technical details on the gate infidelity in particular its dependence on the state of the bus mode, the driving pulse Υ_p and the number of ions.

C.1 Gate infidelity

The set of functionals $\{\mathfrak{F}\{\odot;\bullet\}\}$, that characterize the gate fidelity, can be expressed as

$$\begin{aligned}
\mathfrak{F}\{f;\mathbb{I}\} &= \frac{2\pi i}{\omega} g_1 \,, \qquad \mathfrak{F}\{ff;\mathbb{I}\} = \frac{-2\pi}{\omega} g_1^2 \,, \\
\mathfrak{F}\{fff^*;\mathbb{I}\} &= -i\frac{2\pi}{\omega}(g_2 - 2f_1 g_1 - |g_1|^2 g_1) \,, \\
\mathfrak{F}\{ff^*;\mathbb{I}\} &= \frac{2\pi}{\omega}(f_1 + |g_1|^2) \,, \\
\mathfrak{F}\{fff^*f^*;\mathbb{I}\} &= \frac{2\pi}{w}(f_2 - 4\Re g_2 g_1^* + |g_1|^4 + 4f_1|g_1|^2) \,.
\end{aligned}$$

in terms of the functions

$$\begin{aligned}
g_1 &= \sum_{i=1}^{m} \frac{c_i}{i} \,, \qquad g_2 = \sum_{ijp=1}^{m} \frac{c_i c_j c_p^*}{ijp} \delta_{i+j,p} \,, \\
f_1 &= \sum_{i=1}^{m} \frac{|c_i|^2}{i^2} \,, \quad f_2 = \sum_{ijpq=1}^{m} \frac{c_i c_j c_p^* c_q^*}{ijpq} \delta_{i+j,p+q} \,,
\end{aligned}$$

whith the (unitless) amplitudes that characterize the pulse $\Upsilon_p = \sum_{j=1}^{m} c_j \omega \exp(ij\omega t)$.

The matrix ζ whose norm yields the gate infidelity reads

$$\zeta = \frac{\pi}{\omega}(\zeta_0 + \zeta_1) \ , \ \text{with} \ \ \zeta_1 = \sum_{i=1}^{6} \zeta_{1i}$$

and

$$\begin{aligned}
\zeta_0 &= 2f_1(\gamma_+ + \gamma_- + (2\langle\hat{n}\rangle + 1)\gamma_d)M_1 \\
&- 4f_2\gamma_d N(N-1)M_2 \\
\zeta_{11} &= 2|g_1|^2(\gamma_+ + \gamma_- + (2\langle\hat{n}\rangle + 1)\gamma_d)M_1 \ , \\
\zeta_{12} &= 16|g_1|^2 f_1\gamma_d N M_3 \ , \\
\zeta_{13} &= 4\gamma_d(|g_1|^4 - 4\Re(g_1 g_2^*))N(N-1)M_2 \ , \\
\zeta_{14} &= 4\Re(g_1^2\langle a^2\rangle)\gamma_d M_4 \ , \\
\zeta_{15} &= 8\Re(g_1|g_1|^2\langle a\rangle)\gamma_d M_5 \ , \\
\zeta_{16} &= 4\Im(g_1\langle a\rangle)(\gamma_+ - \gamma_- + \gamma_d)M_6 \ .
\end{aligned} \tag{6}$$

The matrices M_i read

$$M_1 = \begin{bmatrix} -N & 0 & -\sqrt{\Gamma_2} & 0 & 0 \\ 0 & 2\Gamma_1 & 0 & 0 & 0 \\ -\sqrt{\Gamma_2} & 0 & 0 & 0 & 0 \\ 0 & 0 & 0 & 0 & 0 \\ 0 & 0 & 0 & 0 & 0 \end{bmatrix} ,$$

$$
\begin{aligned}
M_2 &= \begin{bmatrix} 1 & 0 & \sqrt{\Gamma_2} & 0 & -3\sqrt{\Gamma_4} \\ 0 & 0 & 0 & 0 & 0 \\ \sqrt{\Gamma_2} & 0 & -2 & 0 & 0 \\ 0 & 0 & 0 & 0 & 0 \\ -3\sqrt{\Gamma_4} & 0 & 0 & 0 & 0 \end{bmatrix}, \\
M_3 &= \begin{bmatrix} -(N-1) & 0 & -\sqrt{\Gamma_2}(N-1) & 0 & 3\sqrt{\Gamma_4} \\ 0 & 0 & 0 & 0 & 0 \\ -\sqrt{\Gamma_2}(N-1) & 0 & 2(N-1) & 0 & 0 \\ 0 & 0 & 0 & 0 & 0 \\ 3\sqrt{\Gamma_4} & 0 & 0 & 0 & 0 \end{bmatrix}, \\
M_4 &= \begin{bmatrix} 0 & 0 & \sqrt{\Gamma_2} & 0 & 0 \\ 0 & N & 0 & 0 & 0 \\ \sqrt{\Gamma_2} & 0 & 0 & 0 & 0 \\ 0 & 0 & 0 & 0 & 0 \\ 0 & 0 & 0 & 0 & 0 \end{bmatrix},
\end{aligned}
\tag{7}
$$

$$
\begin{aligned}
M_5 &= \begin{bmatrix} 0 & \sqrt{N}(N-1) & 0 & 3\sqrt{\Gamma_3} & 0 \\ \sqrt{N}(N-1) & 0 & -\sqrt{\Gamma_1\Gamma_2} & 0 & 0 \\ 0 & -\sqrt{\Gamma_1\Gamma_2} & 0 & 0 & 0 \\ 3\sqrt{\Gamma_3} & 0 & 0 & 0 & 0 \\ 0 & 0 & 0 & 0 & 0 \end{bmatrix}, \\
M_6 &= \begin{bmatrix} 0 & -i\sqrt{N} & 0 & 0 & 0 \\ i\sqrt{N} & 0 & 0 & 0 & 0 \\ 0 & 0 & 0 & 0 & 0 \\ 0 & 0 & 0 & 0 & 0 \\ 0 & 0 & 0 & 0 & 0 \end{bmatrix}.
\end{aligned}
$$

with $\Gamma_p = \binom{N}{p}$. Since ζ_1 vanishes if g_1 (or, equivalently $\mathfrak{F}\{f;\mathbb{I}\}$) vanishes, a large improvement in gate fidelity is achieved even with an only

bi-chromatic pulse that permits to satisfy this constraint. ζ_0 can be reduced only through minimization of f_1 and f_2, and thus will always be finite for a non-vanishing pulse.